Supplementary Materials for

Core and region-enriched networks of behaviorally regulated genes and the singing genome

Osceola Whitney,* Andreas R. Pfenning,* Jason T. Howard, Charles A. Blatti, Fang Liu, James M. Ward, Rui Wang, Jean-Nicoles Audet, Manolis Kellis, Sayan Mukherjee, Saurabh Sinha, Alexander J. Hartemink, Anne E. West,* Erich D. Jarvis*

*Corresponding author. E-mail: owhitney@gmail.com (O.W.); apfenning@csail.mit.edu (A.R.P.); west@neuro.duke.edu (A.E.W.); jarvis@neuro.duke.edu (E.D.J.)

Published 12 December 2014, *Science* **346**, 1256780 (2014)
DOI: 10.1126/science.1256780

This PDF file includes:

Other Supplementary Materials for this manuscript include the following:
(available at www.sciencemag.org/cgi/content/full/346/6215/1256780/DC1)

SUPPLEMENTARY MATERIALS

Core and region-enriched networks of behaviorally regulated genes and the singing genome

Osceola Whitney, Andreas R. Pfenning, Jason T. Howard, Charles A Blatti, Fang Liu, James M.Ward, Rui Wang, Manolis Kellis, Sayan Mukherjee, Saurabh Sinha, Alexander J. Hartemink, Anne E. West, Erich D. Jarvis

This file includes:

Materials and Methods

Supplementary materials section 1

Singing behavior and sample collection. A total of 54 adult male zebra finches that were observed spontaneously singing at least 20 minutes in the morning were individually isolated overnight in sound attenuation chambers. On one of the subsequent mornings for no more than one week, after the lights came on, we collected the brains of males that sang continuously for different amounts of time: 0.5 hour, 1 hour, and every hour up to 7 hours after singing began (n = 6 animals per time point). We only used birds that sang at least >25 bouts per 0.5 hour. We purposely analyzed continuous singing behavior as opposed to acute, as this was the bird's normal behavior, we wanted to maximize gene induction, and if we found differences between time points (as we did), we could still relate them to the start of singing. Silent males (0-hr.) were taken as birds that did not sing within 1-3 hr. for a given morning. We staggered the collection of silent animals, to normalize detecting possible circadian changes in gene expression in song nuclei in the absence of singing. Singing behavior from each bird was digitally recorded for the entire observation time using Avisoft-Recorder (http://www.avisoft.com/). Background cage noises were filtered out using Sound Analysis Pro (http://ofer.sci.ccny.cuny.edu/sound_analysis_pro). After the singing session was complete, whole brains were excised, cut sagittally along the midline, and the separated hemispheres were quickly frozen in a block mold containing tissue-tek (Sakura Finetek, Torrance, CA, USA) and stored at -80° C. Brain sections were cut sagittally at 10 μm and mounted onto PEN membrane glass slides (Molecular Devices, Sunnyvale, CA, USA) for laser capture microdissection (LCM) or Fisherbrand Superfrost Plus slides (FisherScientific, Waltham, MA, USA) for LCM and *in situ* hybridization.

Supplementary materials section 2

LCM, RNA isolation and cDNA synthesis. We established a protocol for preparation of tissue for LCM as reported previously in (*29*) and (*67*). Slides of tissue sections were fixed and sequentially dehydrated in graded alcohols (70%, 95%, 100%, 1 minute each), delipidized in xylenes for 10 minutes, and air-dried for 10 minutes. Under these conditions the fiber density within song nuclei (i.e., Area X, HVC, LMAN, and RA) appears darker than the surrounding

brain tissue (see **Fig. 1B**) when viewed under brightfield on the Arcturus XT Microdissection Microscope (Molecular Devices, Sunnyvale, CA, USA). HVC, Area X, RA, and LMAN were separately microdissected from 7-9 brain sections per bird onto CapSure Macro LCM Caps (Molecular Devices, Sunnyvale, CA, USA). From the captured song nuclei we isolated total RNA using the Picopure RNA Isolation kit according to the manufacturers instructions (Molecular Devices, Sunnyvale, CA, USA), except that the song nuclei on the LCM Cap membranes were carefully removed with RNase free forceps. To stabilize the RNA, the membranes were immediately submerged in 50 µl of RNA Extraction Buffer in a GeneAmp 0.5 mL thin-walled reaction tube (Applied BioSystems, Carlsbad, CA, USA), vortexed briefly, snap frozen in a dry ice ethanol bath, and stored at –80° C.

We evaluated RNA integrity and purity on a Bioanalyzer RNA 6000 PicoChip (Agilent, Santa Clara, CA, USA; 0.5–2.0 ng of RNA from each region depending on its volume). High quality RNA samples were then reverse transcribed and cDNA linearly amplified using the WT Ovation Pico kit (Nugen, San Carlos, CA, USA) or the µMACS SuperAmp Kit (Miltenyi Biotec, Auburn, CA, USA) according to the manufacturer's instructions. With this approach, amplification is initiated at the 3′ end as well as randomly throughout the whole transcriptome. Just before amplification, 10 control transcripts not present in vertebrate genomes from the Agilent One Color Spike-in kit were added to the isolated RNA at multiple concentrations (1:50,000 dilution). These 10 control transcripts vary 6 logs in concentrations, in one log or half log increments and anneal to complementary control oligonucleotides on Agilent microarrays. The spike-ins served as a quality control metric of the amplification and subsequent labeling and hybridization steps. The quality and amount (typically 7–10 µg) of the amplified single-stranded antisense cDNA products were assessed on a Bioanalyzer NanoChip (Agilent, Santa Clara, CA, USA) and a Nanodrop 2000 spectrophotometer (Wilmington, DE, USA). Size of cDNA products ranged between ~50 bases and ~1.5 kb. Amplifications containing artifact peaks in electrophoretic trace were omitted from further processing.

Supplementary materials section 3

Oligonucleotide microarray hybridization. Microarray hybridizations were performed at the Duke Center for Genome Technology Microarray Center. For all amplified samples, 2.2 µg of cDNA were labeled with Cy3 and purified using the Nugen FL-Ovation Cy3 labeling and fragmentation kit (Nugen, San Carlos, CA, USA) according to the manufacturers instructions. After calculation of the degree of labeling (~3%), the Cy3 labeled cDNA was fragmented and hybridized overnight to our custom-designed Agilent zebra finch 4 x 44K oligonucleotide microarray (Agilent catalog# AMADID 022706), as follows. First labeled cDNA was vacuum centrifuged and the pellet resuspended in 25 µl of hybridization solution containing formamide (16%), Nugen F4 Blocking Reagent (31%), Agilent blocking reagent (1X), and Agilent Hyb Buffer (1X). The sample was then denatured at 95^{o} C for 3 minutes and kept at 55° C until each microarray was loaded in a MAUI A4 hybridization chamber (BioMicro Systems, Salt Lake City, UT, USA). A BioMicro Systems A4 clamp was used to secure the microarray slides in the MAUI chambers. Each labeled cDNA sample was then loaded onto a microarray slide and hybridized at 55° C for at least 20 hr. with the humidity chamber positioned over the microarrays. The following day, slides were removed from the MAUI chamber, placed in a slide rack and submerged in Agilent WASH 1 containing 10% TritonX-102 at RT for 1 minute, followed by Agilent WASH 2 at 37° C for 1 minute on a shaker. The microarray slides where then slowly removed from the rack to minimize formation of droplets on the slides and air-dried.

After hybridization and washes, slides were scanned at 5-micron resolution, with a 532PMT=520 setting, on a GenePix 4000B microarray scanner (Molecular Devices, Sunnyvale, CA, USA) and images were saved in TIFF format. The signal intensities of all spots on each image were quantified using the Agilent Feature Extraction Software v.9.5.1 and data saved as .txt files for further analysis.

Supplementary materials section 4

Oligonucleotide microarray design. The zebra finch brain-specific microarrays were designed using transcript sequences from our hierarchically organized brain transcriptome database (www.songbirdtranscriptome.net). At the time of the v.2.1 design (1/23/2009), the database contained sequences of 91,586 transcripts isolated from the zebra finch brain from three sources (*24, 35, 68*). We also included on the microarrays several hundred additional transcripts in the NCBI database from various avian species. The cDNAs were from regular, normalized, and subtracted libraries enriched for transcripts from diverse developmental, pathological, and behavioral states. The 91,586 transcripts were sub-clustered into 43,386 relatively unique transcripts, including splice variants. From these clusters, we selected individual transcripts to design oligonucleotides, based on the quality (required average phred sequence score > 15) and read length (>550 bps). Clones with just 3′ sequence reads were chosen over clones with just 5′ reads, since the 3′ end is often preferentially detected from tissue RNA samples in microarray hybridizations. Some sequences were duplicated as technical replicates to verify microarray quality, yielding a total of 43,838 transcripts. We then filtered out transcripts containing short reads (<150 bps), and put an upper limit of 5 unique transcript variants per gene. This reduced the number of transcripts to 42,304. An additional 1,133 control oligonucleotides or sites were added consisting of multiple concentrations of the 10 Agilent spike in controls described above, GFP, YFP, and dark and bright corner spots placed at strategic locations on the microarray to detect and normalize occasional hybridization artifacts. This resulted in a total of 44,969 oligonucleotide sequences. To these sequences, oligonucleotides (60-mers) were then designed using Agilent's e-array v.5.4 oligonucleotide selection algorithm.

Supplementary materials section 5

Microarray annotation. Oligonucleotides on the microarrays were annotated using both the sequence of the oligonucleotide and the entire transcript sequence from which it was designed, from four sources of evidence: 1) manually curated annotations of ~21,000 transcripts cloned at Duke University by Wada et al. (*24*); 2) PASA software (*69*) to map entire transcripts to the zebra finch genome and test for their overlap with annotated ENSEMBL gene models or for their incorporation into transcript models from other avian and mammalian species (*31, 70*); 3) mapping of the 60-mer oligonucleotide sequences to the zebra finch genome using NCBI BLAST and checking for overlap with annotated ENSEMBL genes using BEDtools (*71*); and 4) applying cDNA transcript sequences from which the oligonucleotides were designed to the human collection of mRNAs in NCBI using BLASTN and the human collection of proteins using BLASTX (*72, 73*). BioMart tools were used to map the human information back to zebra finch genome. A simple evidence-based approach was used to annotate the oligonucleotide based on consensus of this information. After these four procedures, a large portion of the transcriptome still remained unannotated (~40%). Many of these unannotated transcripts had only the 3′ UTR sequenced (*24*), which are known to have poor homology across species, and thus more difficult to annotate than the coding sequence. Therefore, we further examined

transcripts mapping close to ENSEMBL gene models, which often do not have the 3′ UTR annotated. We found that if a cDNA transcript sequence appeared within 3 kb downstream or a 60-mer oligonucleotide sequence appeared within 5 kb downstream of an ENSEMBL gene model, then the consensus annotation (based on other sources) confirmed the mapping of that transcript or oligonucleotide to the upstream ENSEMBL gene more than 70% of the time. A similar relationship existed between ENSEMBL genes and oligonucleotides that mapped to nearby introns within a gene, but not to transcripts that mapped 5′ upstream of ENSEMBL annotated transcription starts. This additional method of annotating oligonucleotides based on mapping near ENSEMBL gene models was included in our evidenced based approach. When the simple majority rule was used, the annotation with the most pieces of evidence was chosen. We manually verified ~100 annotations for each iteration of the above process to determine that they were accurate.

After the annotation, a subset (33,049) of the 43,552 avian oligonucleotides matched 10,092 of the 18,581 predicted gene models by ENSEMBL (v60). The redundancy within the 33,049 transcripts was due to either different oligonucleotides generated against the same transcript, or non-optimal EST clustering, or to different oligonucleotides generated for mRNA variants of the same gene. The remaining 10,503 transcripts on the microarray do not map to ENSEMBL predicted genes. Of these, 44% were found to be potential non-coding RNAs based on an analysis of the ESTIMA zebra finch database (*29*). The annotation information for each oligonucleotide can be found in **Table S1**.

Supplementary materials section 6

Microarray Normalization, Filtering, and Differential Expression. The quality of each microarray hybridization was determined by analyzing the signal distribution with the Bioconductor array quality metrics package (*74*) and outlier microarrays detected using a principle component analysis (PCA) (*75*) and removed usually due to poor RNA sample preparation or microarray quality. The resultant numbers of high quality biological replicates were between 5 and 6 for each time point and song nucleus for all but one time point. The 7 hr. time point of LMAN, which had only three replicates, had to be removed from the analysis due to poor quality. The median intensity of each microarray spot was normalized with variance stabilization (*76*). The data were then log2-fold transformed to better handle some of the large changes in gene expression seen across orders of magnitude. We then filtered out oligonucleotide signals that were not significantly 2.5 standard deviations above the average of the negative spike-in control levels in at least 12 (5%) of the microarrays across song nuclei and birds. This filtering helped reduce the number of variables (transcripts) to compare and ensured we analyzed transcripts that were expressed in multiple animals of a group. To determine if different oligonucleotides measured expression of different splice variants of the same gene, we applied a clustering algorithm to each group of oligonucleotides that mapped to the same symbol or for unannotated transcripts to the same location in the genome. If the correlation of two oligonucleotide measurements across all experiments was > 0.525 (> 2 SDs from the mean of all oligonucleotide correlations on the microarray, estimated $p < 0.02$), the oligonucleotide measurements were merged into one subgroup based on the median. These filtering and merging processing steps resulted in 24,498 oligonucleotide subgroups that represent 9,060 ENSEMBL IDs, and 10,256 unique symbols, which were used for subsequent analysis (**Table S1**). The number of symbols is less than the number of genes, because of multiple splice variants sharing

the same symbol, or because not all transcripts have a symbol due to not being annotated by ENSEMBL. Further, not all symbols have ENSEMBL IDs.

To detect differentially expressed transcripts across song nuclei at baseline, a linear model was created using limma (*66*) to compare every combination of song nuclei against each other in the 0-hr samples. Subgroups with an FDR q-value < 0.1 in any one comparison were determined to be significantly differentially expressed, for a total of 5,167 subgroups. Using a less stringent cutoff, FDR $q < 0.2$ as used for the behaviorally regulated gene expression analyses, resulted in obtaining more differentially expressed transcripts (7,078), but with similar expression profiles (**Figs. 2A vs. S10**); thus, we believe we captured most of the baseline song nuclei gene expression variability at a more conservative FDR $p < 0.1$.

To detect differential expression in response to song production, a linear model, similar to the one described in greater detail in Warren et al. (*29*), was applied to each region independently with two modifications: 1) the behavioral variable, the amount of singing (number of song bouts, number of motifs, number of notes, sum of duration of the vocalizations), was eliminated, as this could bias against finding transcripts regulated by other singing behavioral variables; and 2) an additional indicator variable was included to account for batch effects as well as the time of day the bird was sacrificed, to reduce detection of expression patterns associated with circadian rhythms and experimental variability. In the final model, for each gene we defined the normalized array expression of gene X as:

$$X_n = M + X_tT_t + X_cC_n + X_aA_n + e_n$$

where M is the mean expression of the gene across all microarrays, X_tT_t are factors that represent the time spent singing, X_cC_n represents the time lag of when the bird began singing as well as which batch the experiment was conducted in, X_aA_n are technical RNA amplification factors, and e_n is the residual error of the given microarray.

Supplementary materials section 7

Determining true positive rates for baseline and singing-regulated experiments. We performed an initial verification of the accuracy and reliability of our microarray hybridization and analyses using the well-studied behaviorally regulated gene *EGR1* (*17*). In all brain regions *EGR1* expression measured by our microarray analyses correlated well with the *EGR1* expression measured by *in situ* hybridization on adjacent brain sections from the same animals (**Fig. S2A**). To determine the FDR q-value necessary for an acceptable true positive rate of 80% or higher, we performed *in situ* hybridizations and RT-PCR with 43 and 37 genes, respectively, across each song nucleus ((*24, 33-36, 77*); **Tables S2, S3**). The true positive *in situ* hybridization test for the singing-regulated transcripts included 2 well known positive controls, *EGR1* and *BDNF* (*17, 25*), 15 singing-regulated genes that overlapped with our previous cDNA microarray study (*24*), and 26 new genes identified in this study. The RT-PCR values were calculated relative to a group of 13 negative control genes that did not show regulation on the microarrays.

After applying the linear model described above to each brain region, we observed high true positive rates >87% using a relatively relaxed threshold of FDR q-value < 0.1 for the baseline samples and <0.2 for the singing-regulated samples for all regions but LMAN, where we used <0.1 for the singing-regulated samples (**Fig. S2C,D;** TP in **Tables S2, S3**). The need to use a different cutoff for LMAN was due to the lower number of samples per time point (3 instead of 6). We believe the higher q-value for the singing animals was found because

individual birds sang different amounts, which resulted in higher variable expression for some of the singing-regulated genes compared to the baseline-expressed genes. Our cutoff actually represents a conservative under-estimate of the singing-regulated genes, as there were some false negatives (FN in **Tables S2, S3**). These adjusted p-values, for singing-regulated genes, correspond to stringent non-adjusted p-values of 0.009 for Area X, 0.006 for HVC, 0.006 for RA and 0.002 for LMAN. There was a strong correlation between the microarray and RT-PCR measured expression, with the log-fold change by RT-PCR being ~4 times that of the microarray (**Fig. S2B**).

Consistent with our cutoffs representing a conservative estimate, *EGR1* which is known to be regulated in all four song nuclei, but with weakest up-regulated expression in RA as determined by *in situ* hybridization was identified as regulated in RA on the microarrays with an q = 0.226, slightly below the 0.2 cutoff (**Table S8**). With this stricter analysis (q < 0.2 in one nucleus but close to threshold between 0.2 and 0.5 in any other song nucleus), we still found 1,144 regulated transcripts that showed region-specific enrichment (37% of the transcripts regulated in Area X, 29% in HVC, 41% in LMAN, and 32% in RA; **Fig. S12A, B**).

We also compared the expression of the 1,162 identified transcripts in Area X with prior findings in this nucleus (*24*, *29*, *30*). Wada et al (*24*) identified 31 singing-regulated genes in Area X at the 1 hr. time point using a cDNA microarray, of which we have 14 probes on our array and identified 8 of these using our criteria and FDR cutoff. In Warren et al (*29*), we reported 807 singing-regulated transcripts in Area X between 0.5–7 hr. of singing, which we determine here was represented by 474 genes. Of these, 378 genes (80%) were found among our 1162 singing-regulated genes in Area X. Hilliard et al (*30*) used our microarrays, and found 1364 genes correlated with the act of singing in Area X and 1825 correlated with amount of singing (overlapped by 1132 genes) at the 2 hr. time point. The 1162 genes we report here overlapped the 1364 reported in Hilliard et al. (*30*) only by 230 genes and the 1825 only by 299 genes. These differences are likely due to differences in analytical approaches. Wada et al (*24*) manually identified genes without statistical analyses. Warren et al. (*29*) and Hilliard et al. (*30*) did not experimentally determine a true positive rate of the microarray results, and therefore included regulated transcripts in Area X that likely have weaker associations with singing behavior. The actual number is likely somewhere between our conservative estimate here and the more liberal estimates of these two other studies. Overall, our findings show that determining the true positive rate may be important for obtaining a more accurate assessment of behaviorally regulated genes.

Supplementary materials section 8

Microarray Clustering, Overlap, and Gene Ontology Analysis. We clustered the baseline and singing-regulated genes using several unsupervised approaches: single linkage hierarchical clustering, average linkage hierarchical clustering, and complete linkage hierarchical clustering. The single linkage hierarchical clustering, resulted in a several clusters of very few genes (1–5) and two large clusters containing every other gene. The average and complete linkage clustering yielded similar results, such as the creation of a gene cluster that contains an over-representation of the immediate early genes with a transient expression profile. We chose the average linkage hierarchical clustering to report in the paper since it partitioned the gene expression into coherent and reasonably sized groups after specifying an increasing number of clusters until no new patterns of expression emerged. Using this approach, baseline expression was grouped into k=12 clusters (**Fig. 2A; Table S4**). Adding clusters beyond k=12 did not result in any additional regionally specific profiles, only very similar partitions. The regional and temporal clustering of

singing-regulated transcripts was performed across all regions simultaneously. Every bird was considered a sample and every significant gene-region combination was considered as an item to be clustered. For each pair wise comparison of transcripts x and y, the distance was calculated as 1 – correlation(x,y) where missing data due to comparison across regions was ignored. For the regional patterns, we group the singing-regulated transcripts into clusters of enriched expression in each song nucleus or song nucleus combination. For the temporal patterns in each song nucleus, we grouped the singing-regulated transcripts into k=20 clusters, as is done in Warren et al. 2010. Adding clusters greater than k=20 did not result in any additional regionally behaviorally regulated profiles, only very similar partitions. For determining the minimum number of clusters of singing-regulated genes across all brain regions in one plot (**Fig. 4B**), we used Ward's minimum variance hierarchical cluster method (*78*) to account for missing variables since not all genes were regulated in each song nucleus. Ward's method determines a distance measure between clusters, and merges them based on an optimal value of an objective function.

The expression data shown in the heatmaps of baseline and behaviorally regulated genes represent normalized, log2-fold changes. For each map, each row (across animal samples) was normalized so that the maximum increase was darkest red for an up-regulated gene and the maximum decreases was darkest blue for a down-regulated gene. By normalizing gene expression in this way, we focus on the shape of the gene expression profile, not the log-fold change. Experimental support for this analysis derives from our analysis of *EGR1* expression, where we designed multiple oligonucleotides to measure its expression. The correlation of these different oligonucleotides across experiments (samples) was high, on average 0.97. However, the estimated maximum log-fold change varied between 2 and 4 for different oligos, indicating bias in oligo hybridization. The more 3′ oligos gave stronger signals and fold changes than the more 5′ oligos. This is a typical result in microarray experiments, particularly using laser captured material, where cDNA probe synthesis from the 3′ end is not all full-length up to the 5′ end. Thus, the normalized signal profile of gene expression across samples more accurately reflected how gene expression changes.

To compare baseline expression, region-enriched behaviorally regulated expression, temporal behaviorally regulated clusters, and gene ontology categories to each other, we used a hypergeometric p-value of the overlap. Groups with the number of transcripts overlapping < 5 were removed from the analysis so that small coincidental gene ontology categories would not dominate the results. We ran two comparisons of transcripts to each other: 1) behaviorally-regulated temporal clusters (**Fig. S3A–D**) to behaviorally-regulated regional clusters (**Fig. 4A, B**) using all behaviorally regulated transcripts as the background (**Table S12C**); and 2) temporal clusters (**Fig. S3A–D**) to region-enriched baseline clusters (**Fig. 2A**) using all detected transcripts as the background (**Table S12B**). In addition, we compared gene ontology sets for the region-enriched baseline expression (**Table S6**), region-enriched behaviorally regulated expression (**Table S10A**), and temporal clusters of behaviorally-regulated transcripts (**Table S10B**).

For the gene ontology analysis, we used as background, the genes corresponding to the set of all transcripts detected using the zebra finch brain microarrays, rather than a whole genome set. This is appropriate since these transcripts represent all of the genes we detected in the brain, and the whole genome set predicted by ENSEMBL does not contain all genes representing all transcripts on the microarray. When we use the whole genome as the background set, logically brain-expressed genes dominated the enrichment. The values were corrected for multiple hypotheses by the multtest R package (*79*) because of the large number of ontology sets. The bulk of our gene ontology categories consist of the ontology and pathway categories of the gene

signatures database (*53*). Based on behaviorally regulated hypotheses about what pathways and mechanisms were involved, we added several other functional gene sets to the list outlined in **Table S7**.

Supplementary materials section 9

In situ hybridization. Brain tissue hybridizations were performed as previously described (*24*). In brief, ^{35}S-labeled riboprobes were made from T7 (sense) and T3 (antisense) promoter sites of cDNA clones from two sources used for the microarrays (*24*, *68*), using T7 and T3 RNA polymerases (Roche); cDNAs from the third source (*35*) were not available. Frozen sections were fixed in 3% paraformaldehyde in PBS (pH7.4), acetylated, dehydrated in graded alcohols (70%, 95%, 100%), and air-dried. 120 µl of hybridization solution containing 50% formamide, 10% dextran sulfate, 1X Denhardt's, 12 mM EDTA (pH 8.0), 10 mM Tris/HCl (pH=8.0), 30 mM NaCl, 0.5 µg/µl yeast tRNA, 1 µg/µl polyA, 10 mM DTT, and 1 x 10^6 cpm of ^{35}S-labeled riboprobe was applied to each slide, cover slipped and hybridized in mineral oil overnight at 65° C. Mineral oil and coverslips were removed with rinses in chloroform and then 2X SSPE and 0.1% β-mercaptoethanol at room temp. Slides were then stringently washed in 2X SSPE and 0.1% β-mercaptoethanol for 1 hr. at room temp, 2X SSPE, 50% formamide, 0.1% β-mercaptoethanol for 1 hr. at 65° C, and 0.1X SSPE twice for 30 minutes each at 65° C. Next, slides were dehydrated in graded alcohols (70%, 95%, 100%), dried, and then exposed to BioMax MR film (Kodak) for 2-3 days. The film was processed with D-19 developer and fixer (Kodak). Film images were quantified similarly as previously described (*24*). Briefly, autoradiographic images of brain sections exposed to films were digitally captured using a Dell PC running Olympus DP software to control an Olympus DP71 camera mounted to an Olympus MVX10 microscope. Adobe Photoshop CS3 was used to measure mean pixel intensities on areas of interest after saving the digital image in a tiff format, which allows 16 bits per sampled pixel or 65,535 different shades of gray to be analyzed. Verifications were done with n=2-3 animals per group.

Supplementary materials section 10

Zebra finch RT-PCR. We used real-time polymerase chain reactions (RT-PCR) to verify differential expression of 37 behaviorally regulated transcripts (**Table S3**). The template for RT-PCR was the synthesized cDNA from the LCM dissected song nuclei used in the microarray experiments. RT-PCR was performed using the CFX96 real-time PCR detection system and the SsoFast EvaGreen Supermix kit (BioRad, Hercules, CA, USA). RT-PCR primers for the transcripts of interest were designed from zebra finch exonic sequence using the Roche Universal Probe Library algorithm found online at https://www.roche-applied-science.com/sis/rtpcr/upl/ezhome.html. The 150–400 nucleotide exonic sequence chosen for each RT-PCR target gene overlapped with the oligonucleotide sequence. The primers were designed to have a T_m of ~60° C, and their sizes ranged between 19–25 nucleotides. Corresponding amplicon lengths ranged from 66–76 nucleotides. Reactions for each target amplicon were performed in triplicates. PCR cycling conditions consisted of an initial 30 sec incubation step at 95° C for template denaturation and enzyme activation, followed by 39 cycles of 5 sec at 95° C for denaturation and then 5 sec at 60° C for annealing and extension. This two-step reaction was followed by a melt curve reaction of 65° C to 95° C in 0.05° C increments, to ensure that the desired amplicon was detected. Negative (no template) controls were also performed to verify the reaction was free of contamination. The reaction efficiency for each

target gene was maximized so that cycle thresholds ranged between 20-30. Relative quantification of the RT-PCR amplicons was based on internal reference genes *(B5FY49, CLK4, COX4, DDX50, FAM36A, FAM96B, G3BP2, MRPS14, PSMB1, RPL21, TIM22, TM2D3*) that were not detected as behaviorally regulated by our microarray analysis and fold-differences in expression were based on comparing silent and singing animals using the CFX manager software version 1.6 (BioRad). These negative controls constituted a null distribution that was used to calculate a z-score and significance of each behaviorally regulated gene tested. Besides regulation, the direction of regulation (up or down) was verified before labeling a gene as true or false positive based on this measure.

Supplementary materials section 11

Cis-regulatory motif analysis. The approach to our *cis*-regulatory motif analysis can be divided into three separate steps: 1) score the zebra finch genome using known TF-DNA binding motifs to find 500 bp sequences (motif target windows) likely to be bound by a TF, 2) identify sets of genes that contain high-scoring motif target windows in their non-coding regulatory regions, and 3) find significant enrichments between these "motif target gene sets" and the gene sets defined from analysis of the expression data. We have used this approach in studies of other genomes including human (*80, 81*), honeybees (*82, 83*), wasps, and other insects (*46*).

We began by selecting the set of curated TF-DNA binding motifs to use in this study. We started with a collection of 101 non-redundant vertebrate motifs from the JASPAR (*84*). To it we added 118 vertebrate motifs from the TRANSFAC database (*85*) that corresponded to genes that showed differential expression at baseline (93 motifs) and during singing (63 motifs). These motifs were found by performing a manual search of the TRANSFAC database for every differentially expressed gene that was labeled as a transcription factor by Gene Ontology database. We also included 19 TRANSFAC motifs of transcription factors that have known neural activity-dependent functions, but were not identified in the previous set. From the combined collection was 231 motifs (**Table S14**) we removed redundant motifs (defined as >80% similarity in their motif target gene sets).

For each motif, the genome was scanned in 500 bp windows with shifts of 250 bps. Each window was given an HMM-based score for motif clustering using two methods, STUBB and SWAN (*45, 46*). These programs score a window by integrating over all binding sites in the window, both strong and weak matches to the motif, thereby creating a more rigorous quantification of motif presence than a simple count of sites above a threshold or sum of site strengths, as discussed previously (*45, 46*). For each method, we defined the "target windows" of the given motif as the top scoring 1% of windows in the genome.

The motif target windows were then assigned to genes (called the motif's "target gene set") using two different definitions of a gene's regulatory region. The local "promoter" regulatory region definition includes any window within 5 kb upstream or 2 kb downstream of the annotated start site of a gene model (to allow for annotation errors of the start site and binding sites in the 5′ UTR). The broader "territory" regulatory region definition includes windows contained within (i) the gene body, (ii) upstream of the gene at least 5 kb until half the distance to the next non-overlapping gene, and (iii) downstream of the gene until half the distance to the next non-overlapping gene. To create the motif target gene set, we traversed the list of target windows sorted by motif score, assigning windows to their respective genes based on our regulatory region definitions until 500 distinct genes had been designated as targets.

We identified associations between our motif target sets and gene expression clusters from five analyses; 1) all baseline clusters (**Fig. 2A**); 2) the core set of 97 singing-regulated transcripts (**Table S8, green and yellow highlights**); 3) each section of the Venn diagram for differential singing-regulated expression among song nuclei (**Fig. 4A**); 4) the more strict group of region-enriched singing regulated transcripts (**Fig. S12**); and 5) the temporal patterns of singing-regulated transcripts (**Fig. S3A–D**). The enrichment of the motif target genes in the above clusters was determined relative to the background of all 9,060 ENSEMBL IDs that matched the 18,478 transcripts from the total of the 24,498 transcripts detected in the song nuclei. Before enrichment analysis, the transcripts of these clusters were translated to their corresponding ENSEMBL gene ID based on our annotations (**Table S1**).

To quantify the enrichment of the gene expression clusters with a motif target gene set, we used four different statistics: 1) The first was the one-sided p-value from a hypergeometric test. For each gene expression cluster, 231 statistical tests (one for each non-redundant motifs from JASPAR and TRANSFAC; **Table S14**) were performed and equally many p-values were obtained. 2) Our second statistical measure was the set of q-values (*86*) obtained from these 231 p-values using an R package, which are corrected for multiple hypotheses testing. However, the hypergeometric test used to produce the p-values assumes that all genes in the universe are equally likely to be motif targets. This assumption is violated when using the "territory" method because a gene with a larger territory has a greater chance of being a motif target. 3) Our third approach avoided this assumption by computing a "sampling-based p-value" for each cluster-motif pair. We created a random set of 500 genes by using our motif target set procedure from window with shuffled motif scores, and recorded the size of its overlap with the given gene expression cluster. We repeated this process 1,000 times and report the percentage of times the overlap with random gene sets was greater than the overlap with the actual motif target set as the "sampling-based p-value", our third statistic. 4) Our fourth measure test for motif-gene set associations while accounting for territory length heterogeneity, by computing the "locus length aware Hypergeometric test" (LLHT) p-value described in (*87*).

There are four ways to define a motif's target gene set: two options for window scoring methods (STUBB and SWAN), and two options for assigning target windows to genes ("promoter" and "territory"). For each association between a gene expression cluster and motif to be considered significant, our three p-value statistics (hypergeometric, sampling-based, and LLHT) were required to be at most 0.02, and our hypergeometric test q-value must be at most 0.2 for at least two of the four ways to define the motif target gene set. We note that (i) by using multiple methods for motif scanning, we aimed at improving the sensitivity of our approach, and (ii) by requiring the results of different hypothesis testing procedures to be significant (as well as explicitly imposing a q-value threshold), we hoped to control false positives. Using these criteria, we were able to selectively identify many activated transcription factors that we expected to find enriched in our tan IEG temporal cluster. These results relative to a preliminary Area X study (*29*) where only *CREB* was found in an IEG temporal cluster, highlights our improvements for identifying regulated transcripts and predicting transcription factor binding motifs.

Supplementary materials section 12

*Transcription factor motif-gene cluster networks***.** We used the above enrichment analyses to generate the transcriptional networks that link particular transcription factors to their target genes in clusters of behaviorally regulated genes. One transcription factor or complex can have multiple distinct sequence specificities and conversely different members of the same

transcription factor family can have very similar binding specificities. Thus, to simplify our model, we grouped transcription factor binding motifs together based on their family and the set of proteins that they can bind. For example, the AP-1 transcription factor complex can consist of Fos and Jun proteins as a heterodimer, so we grouped them into several distinct annotated AP-1 class of PWMs. To focus on the highest quality interactions of the network, we restricted our output to cases where at least 3 different transcription factor binding site versions, motif scoring procedures (STUBB or SWAN), or regulatory region definition (territory or promoter) support the interaction. We realize that this biased results towards factors that bind more broadly and have more data available. In the case of AP-1 and EGR1, we found that transcripts on the microarray corresponded to a member of a transcription factor complex that was enriched in a temporal cluster. To look for these examples more systematically, we looked for overlap between the TRANSFAC resource of binding site motifs and all genes on the microarray that were annotated as transcription factors.

To annotate whether a particular edge (transcription factor-cluster relationship) was enriched in a particular brain region, we counted the number of enriched transcripts that came from each brain region (Area X, HVC, LMAN, and RA). That vector was normalized so that the sum of all elements was 1. We then compared that vector to different sets of artificial vectors representing different region specificities. For example, if a transcription factor motif was found upstream of 14 transcripts in a cluster and 7 of those temporal profiles come from Area X and 7 come from HVC, then the artificial vector (Area X = 0.5, HVC = 0.5, LMAN = 0, RA=0) would generated. This vector would indicate the motif-temporal cluster relationship is enriched for the Area X and HVC song nuclei. We labeled a region as enriched for a specific transcription factor motif-gene cluster relationship based on which artificial vector it has the least Euclidean distance to. We then combined all the Euclidean distance results for each region, the network of individual transcripts, and motif gene target predictions, and used them to graphically display the network with cytoscape software v3 (**Fig. S4;** http://www.cytoscape.org/). A simplified collapsed version the network is shown in **Fig. 6C**. The final transcription factor motif-gene cluster network is a visualization of every class of transcription factor binding motifs that are enriched in region (edge) and temporal (node) clusters.

To identify specific binding site locations for identified motif target genes of a cluster, we used PATSER (http://rsat.ulb.ac.be/patser_form.cgi). This program scans a given DNA sequence with a position weight matrix (motif), reporting sites whose log-likelihood ratio score meets a certain threshold.

Supplementary materials section 13

CaRF RNAi knockdown. We cloned a shRNA targeting mouse *CaRF* (5′-GAAGACAGCACCAGCAATTAC-3′) and a control scrambled version of this shRNA sequence (5′-AAACAAGCCCATTCGCGGATT-3′) into the lentiviral vector pLLx3.8 (*88*). Both shRNA constructs were packaged as lentiviral particles in HEK 293T cells (ATCC). The lentiviral RNAi constructs where then transfected into cortical neurons that were dissociated from brains of embryonic day 16 (E16) pups (Charles River Laboratories, Raleigh, NC) and cultured in Neurobasal medium plus B27 supplements. To do this, 5 μM AraC was added on day *in vitro* (DIV) 1 to block glial proliferation. shRNA-expressing lentiviruses were added to the culture medium on DIV1, and by DIV4 infection was estimated at > 80% as judged by GFP expression. Knockdown of *CaRF* was confirmed by quantitative RT-PCR for *CaRF* mRNA. On DIV6, neurons were treated overnight with 1 μm TTX to block neural activity. The next day neurons

were left untreated or they were depolarized for 3.5 hours with 55 mM extracellular KCl, resulting in four groups: 1) a control group expressing scrambled RNAi and depolarized (3 samples); 2) a control non-depolarized group (3 samples); 3) a *CaRF* RNAi knockdown depolarized group; and 4) a *CaRF* RNAi non-depolarized group (3 samples). Total RNA was then purified using RNeasy mini kits (Qiagen, Valencia, CA, USA) and biotin-labeled cRNA was generated following Affymetrix standard protocols. Ten micrograms of the labeled cRNA was hybridized to Affymetrix mouse MOE430 arrays.

All raw CEL from files obtained from the array were processed and normalized on a log scale using RMA Express (*89*). They were then processed to conform to the .gct matrix format with 18 different experiments as columns and 45,101 probes as rows. Gene Set Enrichment Analysis (GSEA) was used to analyze the data with respect to the entire annotated set of genes that represent biologically relevant clusters (*53*). One group of gene sets represented known biological pathways compiled by various online databases. A second gene set was compiled based on having a particular sequence motif representing a transcription factor binding site in the promoter. The default, a signal to noise metric defined as the difference of the means divided by the sum of the standard deviations of the two different groups (*CaRF* control and *CaRF* RNAi) (*53*), was used by GSEA to rank the genes based on differing expression values between the control and *CaRF*-disrupted group. Using other metrics, including t-statistic, available in the program yielded similar results. Genes that ranked in the top 250 in terms of signal to noise metric were studied for further analyses. To calculate the significance of a gene set, such as a pathway or motif, GSEA uses random walk statistics on the ranked list of genes (*53*). For gene ontology analysis we used GOstat (*90*) to look for overrepresented functions on the top 250 and then the bottom 250 genes in this ranking versus the set of entire genes that were ranked in the program. This set is limited to genes that have a corresponding probe on the MOE430_2 microarray and also excludes probes in the microarray dataset that do not have a corresponding gene. In total 14,723 genes were available for this search.

To analyze the microarray data for the creation of the heatmaps (**Fig. 7A,C** and **Tables S16, S18**), we computed a ranked list of *CaRF* knockdown versus scrambled control using a linear model, where the gene expression Y was explained by:

$$Y = A_{SCR} I_{SCR} + A_{KD} I_{KD}$$

where I is an indicator variables with $I_{SCR} = 1$ when the neurons were infected with a scrambled control and $I_{KD} = 1$ in the *CaRF* knockdown samples. $A\_{condition}$ are the estimated coefficients of these variables. To create the heatmap of genes affected by *CaRF* knockdown, the contrast was performed on the A_{SCR} - A_{KD}. The ranked set of activity-regulated gene expression most influenced by *CaRF* knockdown was obtained by creating the design matrix to uncover interactions between knockdown and stimulation in a factorial experiment explained by:

$$Y = A_{KCL} I_{KCL} + A_{KD} I_{KD} + A_{KCL+KD} I_{KCL} I_{KD} + N$$

where I are indicator variables as above, except $I_{KCL} = 1$ when the neurons were stimulated and N is the intercept present in all samples. The variable A_{KCL+KD} is the interaction and used to rank the genes. After the ranked lists were generated, a Wilcox rank sum test (*91*) was used to compare the ranks of transcripts that belong to certain group of singing-regulated genes versus

transcripts that do not. The significance of these values was confirmed by an alternative method (*92*).

Supplementary materials section 14

Collection of H3K27ac ChIP-Seq data.

Adult male zebra finches were isolated in sound attenuated chambers, and their brains were excised after light onset and 1-2 hr. of either silence (n=18) or singing (n=18). Because we needed higher amounts of DNA for this procedure than RNA for the microarray experiments, we dissected whole song nuclei using a different approach. A razor was used to cut off part of the brainstem to create a flat surface with the forebrain, and the back of the brain (cerebellum region) was mounted against a thin plexiglass wall with Vetbond 3M tissue adhesive, placed on the surface of a Stoelting tissue slicer (Cat# 51415). Then 400 μm coronal thick sections were cut, and the sections placed in cold (4^{o} C, on ice) PBS with a proteinase inhibitor cocktail (Roche USA Cat #11697498001, Indianapolis, IN) in a petri dish. The Petri dish with the sections was then placed under a dissecting microscope (Olympus MVX10), and song nuclei quickly dissected (within 5-15 min) with fine scissors and forceps (Fine Science Tools USA, Foster City, CA). The dissected song nuclei were placed in separate eppendorf tubes, frozen on dry ice, and stored at -80oC until further use.

Punched samples from Area X and RA were each pooled from six birds, resulting in 3 biological replicate groups for each behavioral condition. These pooled brain samples were dounced in 1% formaldehyde PBS buffer and kept at room temperature for 15 minutes, washed twice with cold PBS, then lysed in 200 μL lysis buffer (1% SDS, 10 mM EDTA, and 50 mM Tris pH 8.1). The crosslinked material was sonicated with a Bioruptor (Diagenode, Denville, NJ, USA) with 30 seconds on/off cycles to an average size range of 200-400 bp as visualized by agarose gel electrophoresis. Sonicated supernatants were diluted 10-fold in dilution buffer (0.01% SDS, 1.1% Triton X-100, 1.2 mM EDTA, 16.7 mM Tris-HCL, pH 8.1, 167 mM NaCl) before immunoprecipitation. 6 μL of antibody (anti histone H3K27ac, Abcam Cat #Ab4729, Cambridge, MA, USA) was first incubated with 100 μL of Dynabeads Protein G (Invitrogen Cat. #10004D, Grand Island, NY, USA) for 4 hours at 4° C, then the antibody conjugate was added to 2 mL of lysate for overnight IP. Standard TruSeq adapters were ligated for library preparation using the NEB Library Preparation Kit (NEB 6240S and NEB E7335s, Ipswich, MA, USA) and 50 bp single-end sequencing was performed at the Duke Sequencing and Analysis Core Resource on a Hi-Seq 2000 machine at 30 million reads per sample.

Supplementary materials section 15

Analysis of H3K27ac ChIP-Seq data. The reads from the sequencing experiment were transformed into BFQ format and then aligned to the zebra finch genome (Taeniopygia_guttata.taeGut3.2.4, ENSEMBL version 74, http://www.ensembl.org/) using MAQ v0.7.1 with default parameters (http://maq.sourceforge.net/). The files were then transformed into SAM format, reads that did not uniquely map to the genome were removed, and read number statistics was calculated using SAMTools v1.1 (**Table S20;** (*93*)). We decided not to remove duplicate reads, which are likely to represent H3K27ac signal (*94*). Quality metrics were calculated for each sample relative to input using the phantom tools in the SPP ChIP-Seq package (*95*). Based on the quality metrics of the correlation at the phantom peak and the minimum correlation between phantom peaks, we removed two of the replicates obtained from the RA singing group (**Table S20**). In addition, a 4^{th} sample from Area X singing birds was

removed due to poor signal at true positive enhancers present in all others samples near EGR1, FOS, and other genes (**Table S20**).

Peak calling was performed using both Area X and RA data. We first attempted to call peaks jointly on signal from all Area X and RA samples, as this could improve false discovery rate analysis (*96*). However, using the IDR framework (https://sites.google.com/site/anshulkundaje/projects/idr; (*97*)), we found that these peaks were much more consistent with Area X data than with RA, with 21,367 reliable peaks, at a threshold IDR=0.01, of 21,367 reliable peaks discovered in RA and 47,092 in Area X. These values are consistent with data showing quality metrics were consistently lower for RA samples than Area X (**Table S20**), likely due to the smaller amount of tissue available for this smaller song nucleus. To minimize the Area X bias, peaks were called independently for pooled Area X and pooled RA samples. BEDTools (*71*) was used to take the union of these peaks, at 500 bp resolution. Peaks were called using MACS v2.1 (https://github.com/taoliu/MACS/) with parameters "-g 1e9 -p 1e-2 --nomodel --shiftsize 73 -B –SPMR --keep-dup all". To only keep the highest quality peaks, where quantitative differences could be measured, we used a stringent p-value threshold of 1E-5. MACS2 was also used to build log-likelihood files of signal compared to noise for pooled Area X samples and pooled RA samples with parameter "-m logLR -p 0.0001".

In total, 35,958 peaks were identified. BEDTools was used to map peaks to the nearest transcription start site based on ENSEMBL gene models (v74). 15,471 peaks were found within 10kb of the transcription start and likely represent promoter and promoter flanking regions (*98*). The rest of the peaks most likely correspond to enhancers or promoters of unannotated genes. Reads overlapped 12,245 unique ENSEMBL gene models (v74), with 6,575 peaks overlapping exons and 7,574 peaks overlapping introns only.

Once peaks were called, we used the read counts within peaks to determine differential H3K27ac activity between Area X and RA. HT-Seq v0.6.1 (http://www-huber.embl.de/users/anders/HTSeq/) was used to count the number of reads that overlapped each peak (parameter "-m union"). To minimize noise from the lowest quality samples and lowest read number samples, we merged several samples together to create 1-2 groups per brain region/behavior category (**Table S20**). Analysis of Area X – RA differences based on read count at each H3K27ac peak was performed using DESeq2 (*99*). A negative binomial model comparing all Area X groups to all RA groups revealed large scale differences between brain regions with 10,749 peaks enriched in Area X and 7,673 peaks enriched in RA (FDR < 0.01). Surprisingly, at the same threshold, a model that compared singing to non-singing groups yielded 0 significant peaks. Although previous groups have reported a change in H3K27ac in response to neural activity (*58*), the changes were relatively modest and in response to a stimulus many times stronger than one would expect *in vivo*.

To relate the set of transcripts differentially expressed across brain regions at baseline to the difference in nearby H3K27ac peaks at baseline, we compiled a set of scores for each transcripts based on its annotated ENSEMBL gene. We collapsed multiple peaks into one value per transcript by taking the mean of the difference between Area X and RA H3K27ac signal for every peak that mapped to the ENSEMBL gene (**Tables S21, S22,** "Peak Mean LFC" column). We also used an alternative approach of assigning each transcript to the most significantly different peak between regions that mapped to its ENSEMBL ID (**Tables S21, S22, "**Best Peak LFC" column). For each transcript differentially expressed at baseline, we also estimated its specificity for Area X and RA using a linear model. The model estimated the genes differentially expressed at baseline (SM6), and estimated coefficients for Area X expression and for RA

expression. We ran a contrast test using only these two brain regions to estimate the significance and log-fold difference for RA vs. Area X gene expression (**Table S21,** "Expression logFC" column). Once the log-fold change and significance of histone acetylation and expression had been compiled, we used three methods to compare differences in gene expression to differences in H3K27ac signal. First, was the correlation between expression log-fold change and H3K27ac log-fold change, which were strong ($R=0.57$, $p << 0.00001$). Second, we examined the distribution in H3K27ac signal for Area X-specific, RA-specific, and non-specific transcripts (**Fig. 8A**). Third, we computed the significance in the overlap between region-enriched genes and region-enriched peaks using a hypergeometric test, where each gene was mapped to the most significant nearby peak.

To determine genes that were significantly differentially induced between Area X and RA, we developed a more detailed statistical model for these two regions alone. The normalization procedures used were the same as above, except batch effects were subtracted based on a linear model built from all regions, as opposed to each region independently as above (SM6). Using this normalized data matrix, we compared the probability of a gene following a late-response profile in RA vs. Area X with the methods described below. To develop an unbiased model of late/slow response genes, we used the set of behaviorally regulated genes in each region (**Table S8**) for a principal component analysis. Consistent with our previous findings (*24*), we found the first two principal components corresponded to an IEG profile and to a late/slow response profile (**Fig. S8A, B)**. The principal component representing the late/slow response was used as the basis for a linear model, which estimated a coefficient and a probability for a transcript that it followed the late/slow profile:

$$X_n = M + X_{LRG\_AX}A_{LRG\_AX} + X_{LRG\_HVC}A_{LRG\_HVC} + X_{LRG\_LMAN}A_{LRG\_LMAN} + X_{LRG\_RA}A_{LRG\_RA} + X_{IEG\_AX}A_{IEG\_AX} + X_{IEG\_HVC}A_{IEG\_HVC} + X_{IEG\_LMAN}A_{IEG\_LMAN} + X_{IEG\_RA}A_{IEG\_RA} + X_aB_n + e_n$$

where M is the mean expression of the gene across all microarrays, X_aB_n are technical RNA amplification factors, and e_n is the residual error of the given microarray. The A are subscripted by the brain region and by whether they represent the immediate early gene (IEG) or late/slow response profile (LRG). This model identified 702 transcripts that had a positive coefficient (meaning increasing) and also had the most significant match to a late/slow-response profile in any brain region. Next, using the limma package (*100*), we performed a contrast analysis, which compared the estimated Area X coefficient to the estimated RA coefficient to classify the late response gene as Area X enriched, RA enriched, or neither (**Fig. S8C; Table S22**).

Once these statistics had been compiled, the same three methods that were used to examine H3K27ac to gene expression at baseline were used to compare H3K27ac levels to differences across brain regions during song production. The correlation between H3K27ac differences at baseline and relationship of the transcript to the LRG profile had a strong correlation ($R=0.37$, $p=1.6E-12$). The less significant p-value was due to the smaller number of late/slow response genes (**Table S22**) as well as the lower correlation. Second, we examined the distribution in H3K27ac signal for Area X specific, RA specific, and non-specific late-slow response transcripts (**Fig. 8B**). Finally, we computed the significance in the overlap between region-enriched genes and region-enriched peaks, where each gene was mapped to the most significant nearby peak ($p=5.9E-22$ Area X, $p=0.0016$ RA).

For the identified transcripts that had differences in H3K27ac nearby, but were not differentially expressed at baseline, and only differentially regulated during song production in

Area X (**Table S22, blue highlight, 46 genes)** we performed an ingenuity pathway analysis (Qiagen Ingenuity Systems, Redwood City, CA, USA). There were not enough RA genes present for the same analysis (**Table S22, red highlight, 10 genes**).

Supplemental figures

Fig. S1. Experimental design for capturing time series gene expression and behavior. (**A**) Schematic of experimental design of LCM samples isolated from the 4 brain regions (H: HVC, L: LMAN, R: RA, and A: Area X) and hybridized to microarrays in animal replicates of silent (0) or singing for different periods of time (0.5–7 hr.). As a result we analyzed over 200 total microarrays. (**B**) Amount of singing zebra finches performed in time windows of 20 minutes quantified by measuring the number of seconds the bird was in the act of producing song in that window. Rows correspond to birds while the 200 time periods measured are along the x axis. Every bird is normalized so that the maximum amount of singing performed in a window is dark red and the minimum is dark blue. Data organized based on time of day. (**C**) Same data as in (B), but organized based on when the bird was sacrificed. In most birds, there is an initial burst of high rates of singing followed by a steady state of bouts of singing throughout the day. The actual rates varied from 0 to ~100 bouts per 30 minutes, with a mean of 31 bouts per 20 min and standard deviation of 24.

Fig. S2. Microarray gene expression verification. (**A**) *In situ* hybridization measures of *EGR1* (y-axis) relative to microarray measures from individual silent and singing animals from (x-axis) all 9 time points. Fold changes of *EGR1* expression measured by *in situ* hybridization correlates well microarray expression levels (regression statistics in each graph). The two approaches differed in the relative relationships, with Area X having the highest dynamic range in the microarray signal and RA the lowest, which we believe is due to differential sensitivity of expression level differences among song nuclei by the two methods. (**B**) Real time PCR analysis of baseline and singing-regulated genes**.** These genes were all measured from the 0, 1, 2, or 3 hr. time points, at various microarray significance levels, from each song nucleus, with most from Area X (37 genes). Samples from the same time point were pooled. Despite confounding factors such as different microarray hybridization efficiencies for different genes and sample pooling that occurs for the RT-PCR data, but not the microarray, the quantitative analysis shows a strong correlation between RT-PCR and microarray-measured expression levels. The overall log-fold change is calculated as the difference between a gene's log-fold change and a control group of 13 non-regulated genes during singing (SM10). The log-fold change predicted by the RT-PCR is four times that of the microarray. (**C**) True positive analyses of microarrays for differential gene expression detected at baseline (in silent animals) evaluated by *in situ* hybridization. (**D**) True positive analyses of microarrays for singing-regulated genes evaluated by a combination of *in situ* hybridization and RT-PCR. The inset table summarizes genes tested for each region by true positives (TP), false positives (FP), and TP rate = 1 – #TP/(#TP + #FP). The information used for the calculation in panel (C) is found in columns F–I of **Table S3**. The results of the individual genes tested are in **Table S2** for baseline and **Table S3** for singing-regulate genes.

Fig. S3. Temporal-regional singing-regulated gene expression across song nuclei. (**A–D**) Heatmaps of all 2,740 singing-regulated transcripts, hierarchically clustered first into 20 temporal patterns (colored boxes on left), then separated out by song nucleus (each panel), then by first time point of increased or decreased expression, followed by level of significance from

highest to lowest in the linear model (local row separation). This means, for example, that the blue cluster (top color of each panel) is a group of transcripts with late sustained increased expression starting at 2–3 hr. after singing, with the majority of the transcripts with this temporal pattern belonging to Area X and HVC. Red: increases; blue: decreases; white: no change relative to 0-hr. samples. Average expression levels of genes in each of the 20 clusters across time is shown in **Fig. 5**.

Fig. S4. Full network of singing-regulated transcription factors and predicted binding target relationships summarized in Fig. 6C. Directed edges represent the predicted binding of a transcription factor (diamond) to target genes (circles). Node color reflects membership in a temporal cluster of singing-regulated transcripts in **Figs. 5 and S3**. The edge color represents the brain regions specific for the temporal profile of the transcripts identified (blue, Area X; green, HVC; yellow, LMAN; red, RA; black, multiple brain regions). Singing-regulated transcription factors that are also targets of EATFs, such as *EGR1* (EGR1-s1 transcript) and *AP1* (FOSs transcript), are labeled by diamonds and colored by their corresponding temporal cluster.

Fig. S5. Global properties of transcription factor binding sites. (**A**) Heatmap of binding site score and the associated genes containing the seven dominant transcription factor binding sites (x-axis) found in genes of the tan temporal cluster, compared to the genes with the same binding sites in other clusters (y-axis). Each row represents an ENSEMBL gene corresponding to a transcript in the cluster indicated (y-axis color on the left). Each column represents a transcription factor binding motif, including known alternative versions of it, that was used to scan the genome; the darker the shade of blue, the higher the motif score found for the gene. No bar means no binding site found. All motif scoring methods and regulatory region definitions are combined using the maximum value. Along the right of the heatmap is the smoothed averaged motif score found per ENSEMBL gene. A stronger enrichment in the tan immediate early gene cluster can be seen. (**B**) Relationship between transcription factors and gene clusters differ across brain regions. Rows represent the edges found (shown in **Fig. 6C**) between transcription factors and putative target genes in singing-regulated clusters based on temporal pattern. The intensity in a cell of the heatmap is proportional to the number of transcripts from a particular brain region (columns) that comprises the significant relationship between transcription factor and target. Average linkage hierarchical clustering was used to create the dendrogram of regions above the heatmap. The dendrograms shows that the transcription factor-motif relationships recapitulate the known relationships of brain anatomy, as do the baseline gene expression patterns (**Fig. 2B**)

Fig. S6. Gene expression of the NFE2L1 and MAF transcription factors in song nuclei at baseline in the absence of singing. The two genes are known to bind their recognition site in a heteromer complex (*52*). The plot is extracted from the baseline values and clustering of **Fig 2A**, and ordered the same as **Fig. 2A**. The left dendrogram are the clusters (blue cluster, higher in pallial song nuclei relative to Area X; white cluster, no difference in Area X; turquoise, higher in Area X relative to pallial song nuclei). To the left of the dendrogram is the heatmap of the log-fold change in expression of 6 different NFE2L1 and MAF transcript variants (rows: MAF-s1-4; NFE2L1-s1-2) of each animal (columns) normalized to the mean values of Area X (similar to **Fig. 2A**). Three variants are higher in HVC, LMAN, and RA, and one lower. The 6 transcripts are clustered using average linkage hierarchical clustering (dendrogram); red, increased

expression relative to the average of Area X; blue, decreased expression relative to the average of Area X.

Fig. S7. Genes in specific molecular pathways of neurons affected by *CaRF* knockdown. (**A**) The "St WNT Ca2+ Cyclic GMP Pathway". (**B**) The "GABA Pathway". The affected pathway genes were detected by GSEA (*53*) as enriched genes decreased in the *CaRF* knockdown cells independent of membrane depolarization. The x-axis list the rank order of the gene transcripts detected by ~45,000 oligos. The y-axis show three plots: the rank metric for highest (>0) to lowest (<0), if a gene is part of the specific pathway highlighted (blue lines), and the contribution of those genes to a cumulative increase of the enrichment score (red line) that is used calculate the significance of the gene set. A bias towards increase or decrease can be found based on the maximum value of the red/blue lines. The strength of the increase or decrease of each gene at a particular ranking is shown in gray.

Fig. S8. More stringent clustering of RA and Area X singing up-regulated genes. (**A**) First principal component of all singing-regulated genes for each song nucleus, which contains many immediate early genes. (**B**) Second principal component of all singing-regulated genes for each song nucleus, which corresponds to the late/slow response genes. Principal component scores for each region (bar colors) are averaged at each time point. The scores are normalized such that the maximum value is 1 and direction is consistent across brain regions. Error bars show standard deviation for each time point. (**C**) Heatmap profile of transcript levels that most significantly match the late response principle component, with red representing an increase and blue representing a decrease during song production. The gene expression values are normalized such that the maximum is 1 and non-singing birds at 0. Transcripts are organized based on whether they have a significantly ($p < 0.05$) better match to the Area X (blue row labels), RA (red column labels), or neither (black column labels) cluster. Boxes highlight the region-specific upregulated genes.

Fig. S9. Plot of H3K27ac peaks of example genes in Area X vs RA before and after singing. (**A**) FOS has peaks in both RA and Area X, and known to be regulated at higher levels in Area X by singing, but neither nucleus shows a significant difference in peaks before and after singing. (**B**) PTPN5 regulated in Area X also shows no peak difference before and after singing. (**C**) A comparable result is seen for BDNF in RA before and after singing. (**D**) A late response gene IL1R1 in RA shows no large difference. (**E**) CALB1 a gene that marks Area X with higher levels early during development (*101*) and shows a further late-response singing increase in Area X also shows no detectable difference in peaks before and after singing. ENSEMBL gene models are at the bottom of each panel. Plots in (D) and (E) were displayed using different software.

Fig. S10. Plot of H3K27ac peaks of behaviorally regulated genes in Area X vs RA before and after singing. (**A**) Density plot of immediate early genes (based on temporal profile) upregulated in response to singing in RA vs Area X and the difference in the level of nearby H3K27ac peaks in the genomes of the cells in RA X vs. Area X. Each H3K27ac peak is mapped to the nearest transcription start site of the gene. For each gene, the change in all mapped H3K27ac peaks are averaged. Genes are separated into three categories, no enrichment in RA vs. Area X (grey), enriched in Area X (blue) and enriched in RA (red). (**B**) Similar to A, but showing the density of H3K27ac peaks between RA vs. Area X for downreglated late-response

singing-regulated genes. Only Area X shows a weak relationship. (**C**) Similar to A, but showing the density of H3K27ac between singing and non-singing in Area X. Immediate early genes that increase in Area X are shown in green, while other genes regulated in Area X are shown in gray.

Fig. S11. Region-enriched gene expression at baseline with a less stringent FDR q < 0.2. A total of 7,078 transcripts (rows) are detected as differentially expressed across regions at baseline in silent birds. Note the similarity of expression clusters found at FDR q < 0.1 (**Fig. 2A**). Red, increases; blue, decreases; white, no change relative to mean Area X expression. Each column is an animal replicate. Mean expression in each region was used to generate a small average linkage hierarchical tree, representing the molecular expression relationships of the brain regions to each other.

Fig. S12. More stringent region-enriched expression in response to song production. (**A**) A 4-way Venn diagram showing region specific enrichment of the more strict set of 1,144 transcripts (FDR q < 0.2 in region of interest, FDR q > 0.5 in other regions). (**B**) Heatmap of all 1,144 region-enriched transcripts from the stricter Venn diagram (FDR q < 0.2 in region of interest, FDR q > 0.5 in other regions). Each transcript is normalized so that the maximum increase relative to non-singing birds in any region is the darkest shade of red for increasing transcripts and the maximum decrease is the darkest shade of blue for decreasing transcripts. Detailed results are in **Table S8**.

Supplemental table legends

Table S1. Annotations of oligos and corresponding transcripts on the songbird 44K microarray. Listed items include oligo ID (column **A**), Duke cDNA ID (**B**), ESTIMA ID (**C**), NCBI Accession # (**D**), ENSEMBL ID when available (**E**), the source (**F**) of the original DNA sequence (0= Wada et al 2006(*24*); 1= Li et al 2007(*35*); 2 = Replogle et al 2008 (*68*)), whether the RNA is coding [0] or non-coding [1] (**G**), and the oligo nucleotide sequence synthesized on the array (**H**). Also shown are the final gene symbols **(I**) and gene description (**J**) used for analyses. The evidence that led to that final symbol and description is summarized (**K**). All symbols from the various methods of annotation are listed as well (**L**). Evidence for the annotations are in columns M through V. o, oligo; p, pasa defined annotations of clustered transcript sequence reads against the zebra finch genome. If a transcript representing a gene does not have a functionally identified name, then simply its pasa or clone ID was used as the gene name in columns I and J. The order of features (oligo and control spots on the array) is in the same order as listed adjacent to column A (available online).

Table S2. List of genes used to validate baseline expression with *in situ* hybridizations. The expression values (columns **G-J**) are the normalized levels from the microarray experiment (SM6). The *in situ* hybridization results (columns **K-N**) are scored either as true positive (TP), false positive (FP), false negative (FN), or true negative (TN) The sources of *in situ* hybridizations (**column E**) are Li et al (*35*), Lovell et al (*36*), Velho et al (*102*), George et al (*77*), Wada et al (*24*), Kubikova et al (*34*) or this study, (available online).

Table S3. List of genes used to validate singing-regulated expression by *in situ* hybridization and RT-PCR. The table has five sections: 1) Gene Information; 2) Verification

Summary; 3) Microarray Information; 4) *In situ* Hybridization Information; and 5) RT-PCR Information. Verifications are of three varieties: *in situ* hybridization only (39 transcripts, cyan colored), *in situ* hybridization and RT-PCR (4 transcripts, blue), and RT-PCR only (33 transcripts). The gene information includes the specific cDNA clone ID that was tested (column **C**) and the corresponding transcript variant (column **D**). The verification summary section brings together both the *in situ* hybridization data and RT-PCR data and was used to calculate the final true positive (TP, green) and false positive (FP, red) rates as in (**Fig. S2D**). In addition, the table also shows false negative (FN, orange) and true negative (TN, light green) findings (columns **F-I**). These same classifications are used in the *in situ* hybridization (**AB-AE**) and the RT-PCR (**T-W**) sections. The values in the microarray section are FDR q-values, with significant differences highlighted in dark green for each song nucleus at a given time point relative to silent controls (**K-N**; timepoints in column **R** and **Table S8**). In both the *in situ* hybridization and the RT-PCR, gene expression was often measured at more than one time point. The sources of *in situ* hybridizations (**column S**) are Li et al (*25*), Wada et al (*24*), Jarvis and Nottebohm (*17*) or this study, (available online).

Table S4. Transcripts detected in song nuclei in this study. Listed are the 24,498 groups of expressed transcripts detected in song nuclei above the background spike in controls in at least 12% of the microarray samples (i.e. n=4 or more animals). Unique Transcript ID (column **A**) is the name given to the group of transcripts from the same gene that are expressed similarly. s, indicates transcript variant. Other columns show group IDs (**B**), gene symbols (**C**), gene description (**D**), ENSEMBL ID (**E**), zebra finch chromosome (**F**) and number of oligos that generated to the group of transcripts (**G**) with oligo IDs (**H**). For example, there are 8 oligos on the array that recognize transcripts from the glioblastoma amplified sequence (GBAS) gene, and these recognize transcript variants with 4 distinct patterns (GBAS-s1 to s4) (available online).

Table S5. Transcripts differentially expressed in song nuclei at baseline. Listed are the 5,167 transcripts detected as differentially expressed among song nuclei at baseline non-singing activity using a correlation and distance measure (SM8). The unique transcript ID (**A**) identifies the specific transcript and the symbol (**B**) of the gene to which it maps (available online).

Table S6. Functional enrichment data for differentially expressed genes at baseline. Rows are colored according to cluster membership (**A**). The functional categories (**B**) are based on searches of genes categories from different sources, including gene ontology (**C**; source details in **Table S7**). The enriched sets of genes for each category are identified in column E. Rows are color-coded according to baseline-region cluster membership (as in **Fig. 2A**). Rows in bold text are the categories that show the strongest enrichment for each regional cluster, based on number of genes (**D**), p-values based on hypergeometric tests (**F** and **G**), and percent of genes from that cluster showing such enrichment (**H**) (available online).

Table S7. Gene expression sets from prior studies used for comparative enrichment analyses. Listed are the names we have given to the genes sets, their description, numbers, whether the experiments were conducted *in vivo* or in cell culture, and the literature and PubMed ID source of the data (*103-117*) (available online).

Table S8. Transcripts differentially expressed in song nuclei after singing. Listed are the 2,740 transcripts detected as differentially expressed among song nuclei after singing. The unique transcript ID (column **A**) identifies the specific transcript and the symbol (column **B**) the gene to which it maps. The linear model FDR q-values are shown for each song nucleus (**E-F**), as well as the temporal cluster to which the transcripts belong to for each nucleus (**J-M**). NA, not applicable; xReg, regulated by singing. The data are sorted from most to least significant for combinations of the four song nuclei. The core 20 transcripts detected as singing-regulated in all four song nuclei are highlighted in green, and the remainder of the core in three or on the border of four song nuclei are in yellow (available online).

Table S9. Differential singing-regulation of alternative transcript variants. Listed are the differential singing-regulated alternative transcript variants (s1, s2, s3, …) detected by oligos specific to those variants. These variants include those that are alternatively spliced, alternatively started, and alternatively polyadenylated. Of the 2740 singing-regulated transcripts, 390 were differentially-regulated alternative variants from 82 genes. For example, we detected *UNC5A* transcript variant s1 (UNC5A-s1) as regulated by singing in Area X, but transcript variant s2 (UNC5A-s2) as regulated in LMAN. Group ID is the ENSEMBL gene ID based on genome mapping; the singing-regulated brain region cluster is from the temporal clusters (available online).

Table S10. Functional enrichment data for singing-regulated genes. (**A**) Enrichment in regional singing-regulated clusters of transcripts. (**B**) Enrichment in temporal singing-regulated clusters of transcripts. Rows are colored according to cluster membership (column A). The functional categories (column B) are based on searches of genes categories from different sources, including gene ontology (column C; source details in **Table S7**). The enriched sets of genes for each category are in column E. The p-values (columns F and G) are based on hypergeometric test. The % of list (column H) is the percent of transcripts relative to the total number of regulated transcripts for a given region or temporal cluster (available online).

Table S11. Proportions of transcripts among temporal singing-regulated clusters. The Table shows for each the 20 temporal clusters (column **A**) their region-specificity (columns **D-H**). Cluster size (**C**) is calculated as the number of transcripts that make up that temporal cluster. The percentage for each song nucleus (**D-G**) is the percentage transcripts for each temporal cluster that come from that song nucleus. We treated the percentage of transcripts for every song nucleus as a vector. That vector was compared against a vector representing every combination of regions using Euclidean distance to determine the regions enriched (**H**). For example, the vector for tan cluster (0.43, 0.24, 0.2, 0.13) was closest to the vector representing all regions (0.25, 0.25, 0.25, 0.25) as opposed to the vector for Area X (1, 0, 0, 0). As a result, the five clusters that show a strong representation in all regions have at least 10% of their transcripts from each region (available online).

Table S12. Statistical results for hypergeometric tests of overlap of transcripts from the baseline region-enriched, singing region-enriched, and singing temporal-enriched clusters. (**A**) Correlations between baseline region-, singing region-, and singing temporal-enriched clusters. (**B**) Correlations between baseline region- and singing region-enriched clusters. (**C**) Correlations between singing region- and singing temporal-enriched clusters. (**D**) p-values for

baseline region- and singing region-enriched correlations. (**E**) p-values for baseline region and singing temporal-enriched correlations. Red text denotes when the region baseline pattern is correlated with region specific pattern from the same or subgroup of song nuclei (available online).

Table S13. Transcription factor motif enrichment data for temporal patterns of singing regulated gene clusters. Each row represents an association between a temporal singing-regulated cluster and a transcription factor motif (column **D**) from the database in (column **C, Table S14**). Listed is the number of genes in the cluster for which an ENSEMBL annotation was found (column **E**) as well of the number of those genes that were identified as having the motif overrepresented in their non-coding regulatory region (column **F**) by a given method (column **B**). The significance of the association was quantified with four statistics; simulation p-value, hypergeometric p-value, locus length aware hypergeometric test p-value, and hypergeometric q-value (columns **G-J**) (available online).

Table S14. TRANSFAC and CUSTOM scanned binding motifs. (**A**) Listed are 118 binding motif names from the TRANSFAC database that corresponded to transcription factors that were differentially expressed in song nuclei at baseline or during singing. (B) 19 TRANSFAC motifs of TFs we hypothesized to be regulated by neural activity or plasticity. (C) 101 motifs used from the JASPAR database (available online).

Table S15. Enriched motifs in temporal clusters of behaviorally regulated transcripts expanded to individual transcripts. Listed are the transcription factor (column **A**) to target gene (column **B**) relationships predicted by the transcription factor binding site scans that were supported with enrichments between the TF's motif target gene set and the target gene's temporal singing-regulated cluster (column **C**) as shown in **Fig. S3**. The specific brain region enriched expression of the target gene (column **D**) is also listed (available online).

Table S16. Top 100 genes most affected by *CaRF* knockdown. Listed are the top 100 transcripts identified as most differentially expressed between all samples with the scrambled control versus CaRF knockdown in mouse cultured cortical neurons. The subgroup ID (**A**) identifies the specific transcript and the symbol. This is a separate set from the zebra finch IDs. (**B**) Corresponding Affymetrix probe ID. (**C-E**) Gene annotations. (**F-I**) Statistical values calculated for each transcript (available online).

Table S17. Pathway enrichment and gene ontology analysis of *CaRF* effected genes. (**A**) Gene sets built from MSigDB pathways were compared using GSEA (*53*) to the ranked list of genes effected by CaRF knockdown in the absence of membrane depolarization. Genes were ranked by signal to noise ratios using the GSEA default. Listed are name of the enriched pathway, the highest enrichment score, the nominal p-value, false discovery rate (FDR), family wise error rate (FWER), and size or number of genes found in the set. Thresholds for inclusion were $p < 0.05$ and $q < 0.25$. (**B**) Results of a gene ontology analysis (*90*) of the top 250 genes affected by *CaRF* knockdown in the absence of membrane depolarization, also ranked by GSEA according to signal-to-noise ratio ($p < 0.05$) (available online).

Table S18. Top 100 genes whose activity-dependence is most affected by *CaRF* knockdown. Listed are the top 100 transcripts identified as most differentially regulated by KCl membrane depolarization between the scrambled control virus and the *CaRF* knockdown virus infected mouse cultured cortical neurons. (**A**) The subgroup ID identifies the specific transcript and the symbol. This is a separate set from the zebra finch IDs. (**B**) Corresponding Affymetrix probe ID. (**C-E**) Gene annotations. (**F-H**) Statistical values calculated for each transcript (available online).

Table S19. Membrane depolarization- and *CaRF*-regulated genes that overlapped with singing-regulated genes. Listed are 55 genes that were regulated by singing and enriched in zebra finch Area X and HVC, and that showed membrane depolarization and CaRF regulation in cultured cortical mouse neurons. Of these, 9 have a putative *CaRF* binding site in the zebra finch genome (#1 in column **D**). P-values are FDR (available online).

Table S20. Quality control and sample annotation for H3K27ac ChIP-Seq. Each row corresponds to a different sample taken from the RA or Area X regions in silent and singing birds. Input comes from DNA with the H3K27ac antibody (DNA) or from whole cell extract (WCE, Column **E**). Highlighted green values represent quality control measures within a reasonable level of tolerance while red values represent low quality (available online).

Table S21. H3K27ac near genes that are differentially expressed across brain regions at baseline. (**A-D**) Listed are 3,397 transcripts that are differentially expressed at baseline and have at least one H3K27ac peak that maps to it. (**E-H**) The expression t-value, p-value, adjusted p-value, and log-fold change for the expression in RA relative to Area X. (**I**) The "expGrp" classifies the genes as Area X enriched, RA enriched at $p < 0.01$ or neither. (**J**) Mean log-fold difference between in RA vs. Area X for all peaks that map to the gene corresponding to that transcript. (**K, L**) The most significant peak mapping to that transcript and its log-fold difference and category in Area X vs. RA (available online).

Table S22. H3K27ac near genes that are differentially induced across brain regions during singing. (**A-D**) Listed are 346 transcripts that are classified as late-response singing-regulated genes and have at least one H3K27ac peak that maps to it. (**E-H**) The expression t-value, p-value, adjusted p-value, and log-fold change are shown for the match to the identified LRG profile in RA relative to Area X. (**I**) The "expGrp" classifies the genes as Area X enriched, RA enriched, or enriched in neither region during song production ($p < 0.05$). (**J**) The mean log-fold difference between in RA vs. Area X for all peaks that map to the gene corresponding to that transcript. (**K, L**) For the most significant peak mapping to that transcript, listed is the log-fold difference in Area X vs. RA and the peak category. (**M**) The expression category of the gene at baseline, where "Ax" is enriched in Area X at baseline, "Ra" is enriched in Ra at baseline, "diff" is genes that are differentially regulated in one or both of the nidopallial song nuclei, HVC and LMAN, and "none" refers to transcripts that are not detected as differentially expressed at baseline. Highlighted in blue are transcripts not differentially expressed at baseline, but singing-regulated in Area X and have H3K27ac peak in their genes at baseline. Highlighted in red is the converse relationship for RA (available online).

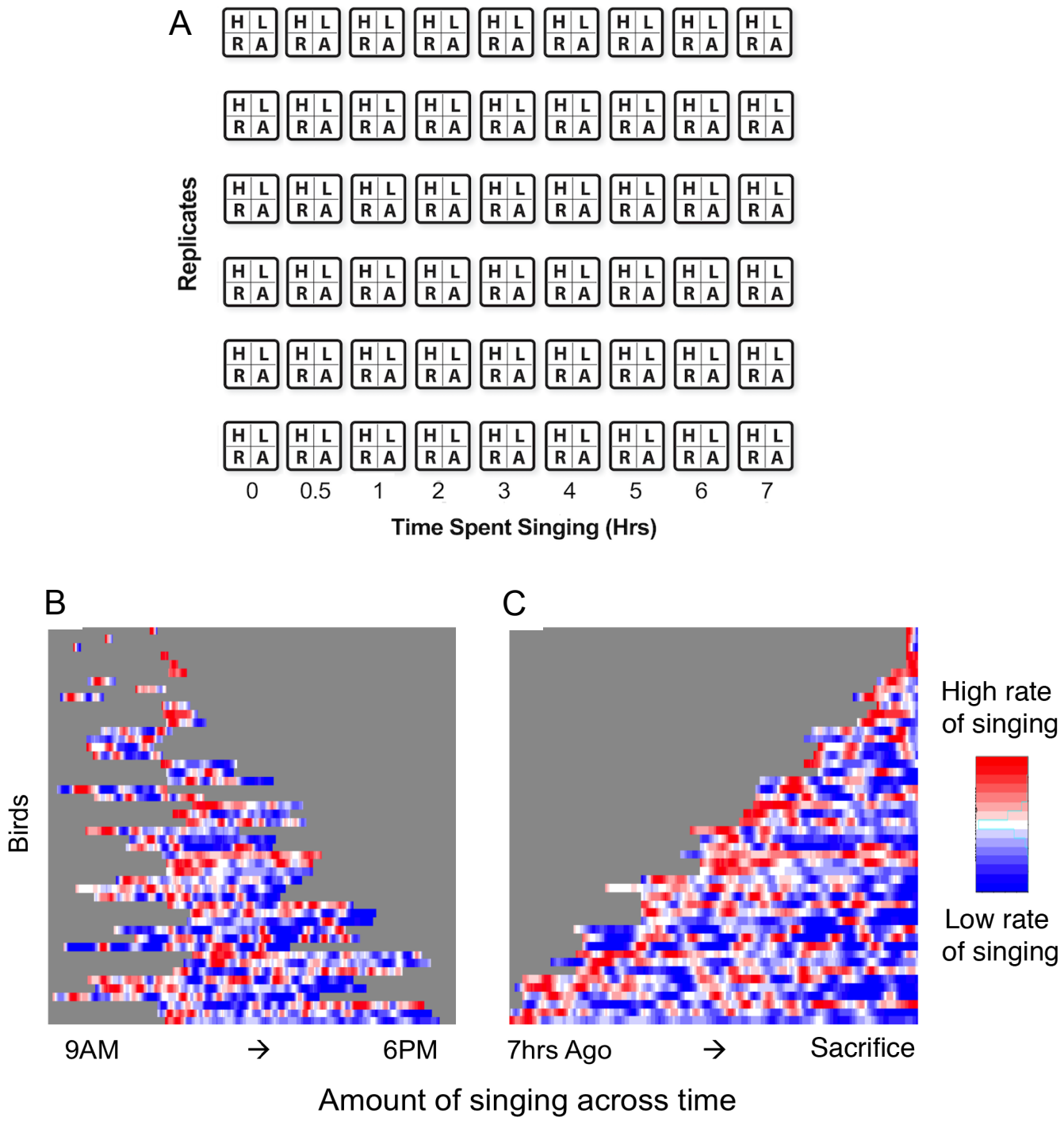

Supplementary Figure S1

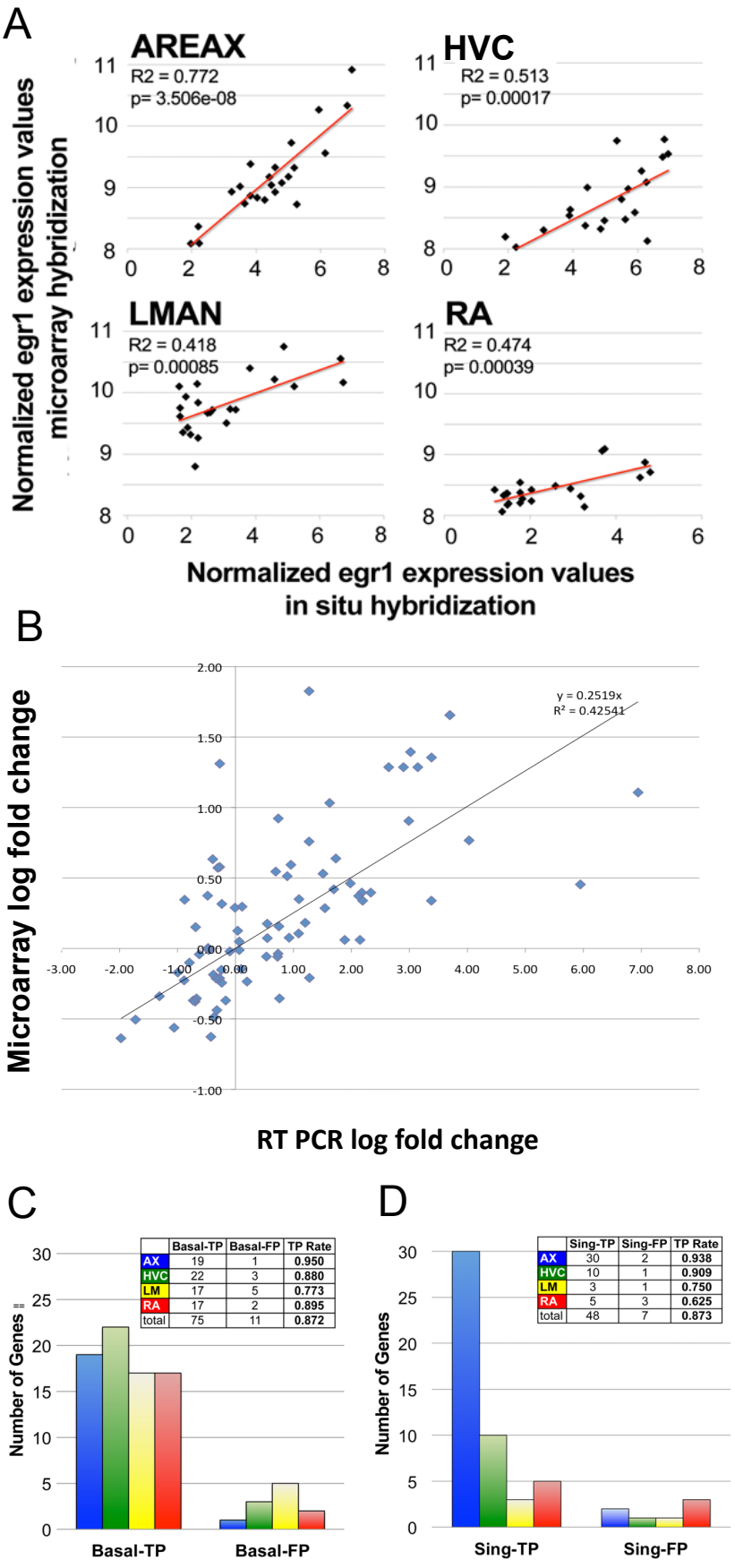

Supplementary Figure S2

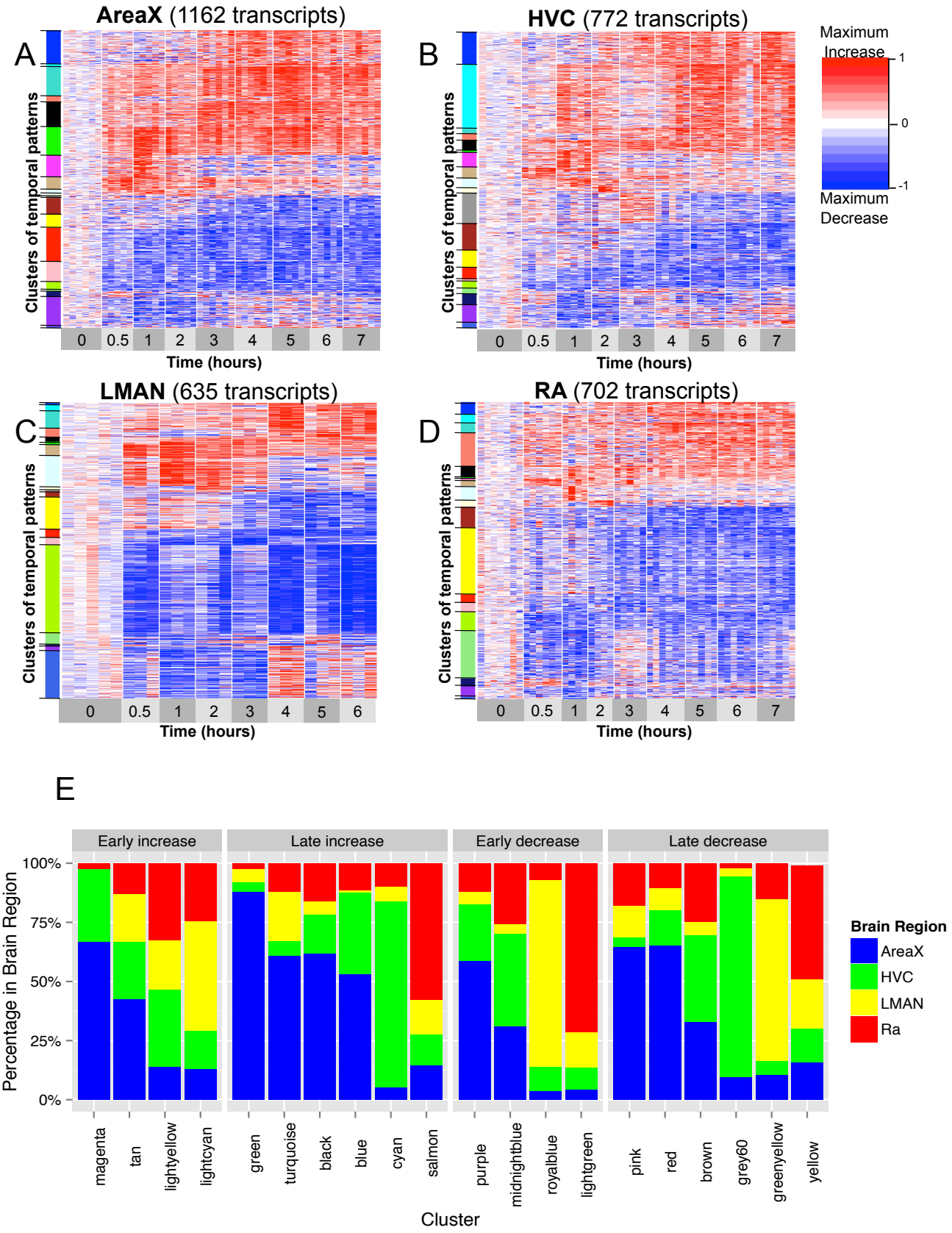

Supplementary Figure S3

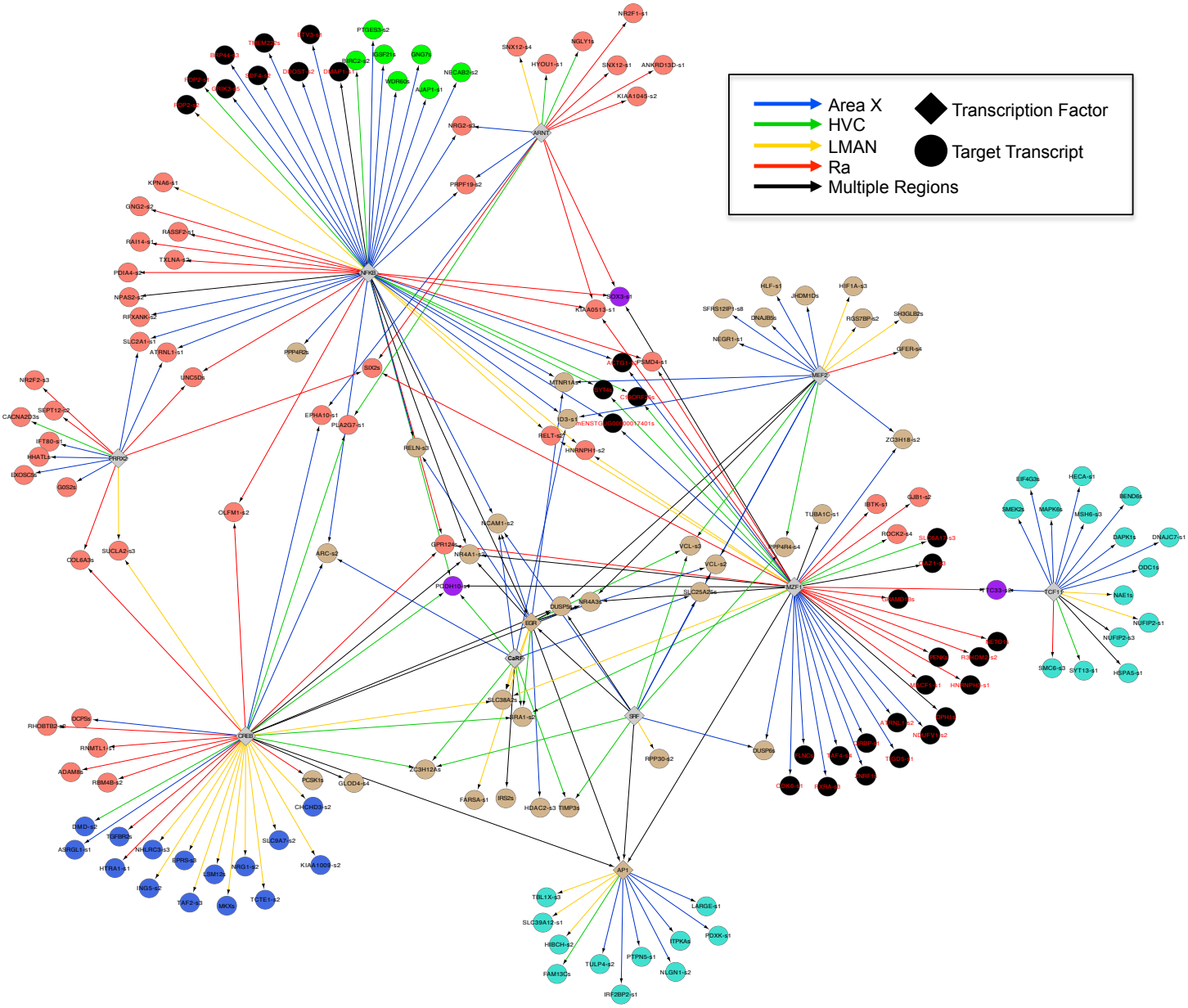

Supplementary Figure S4

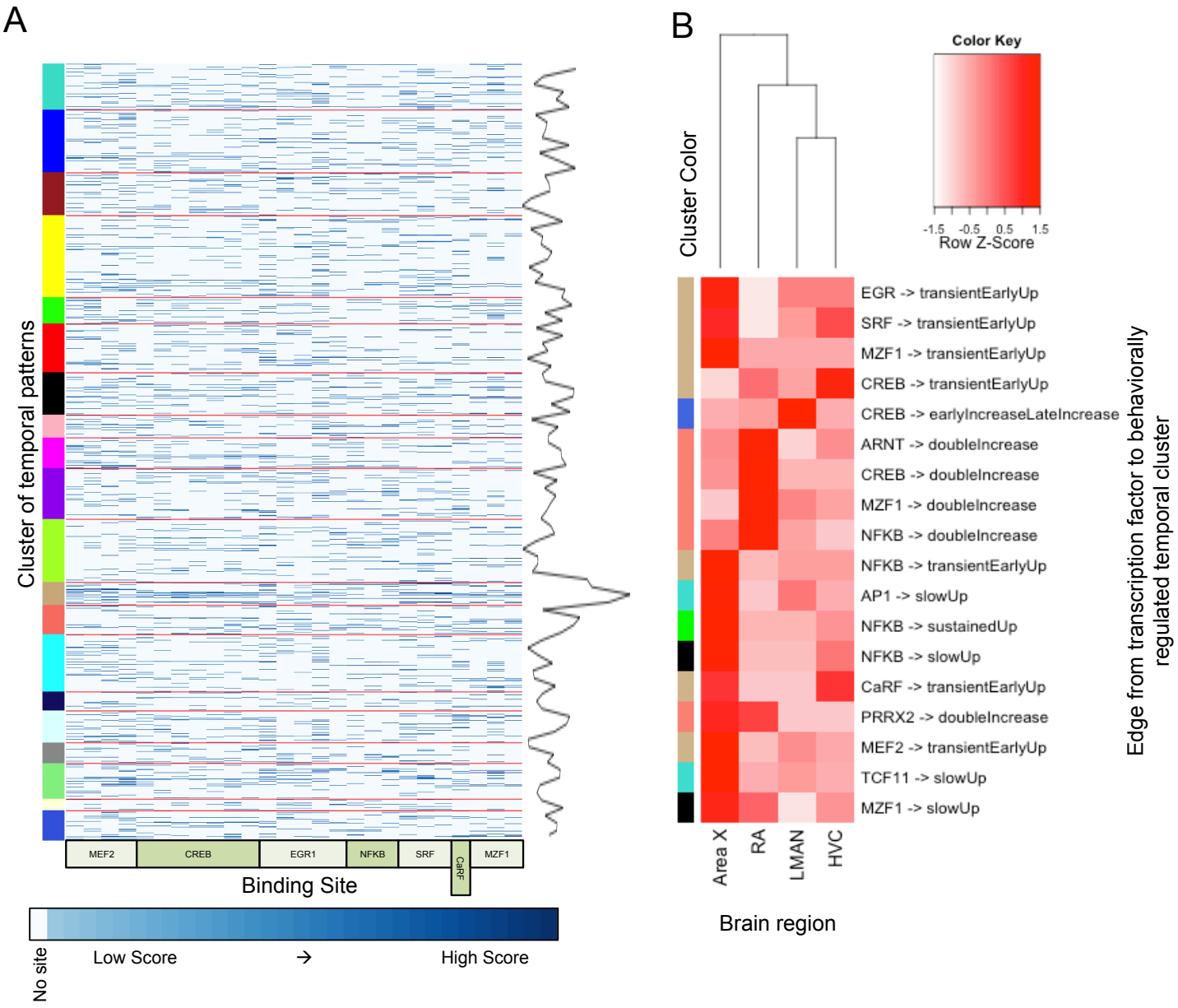

Supplementary Figure S5

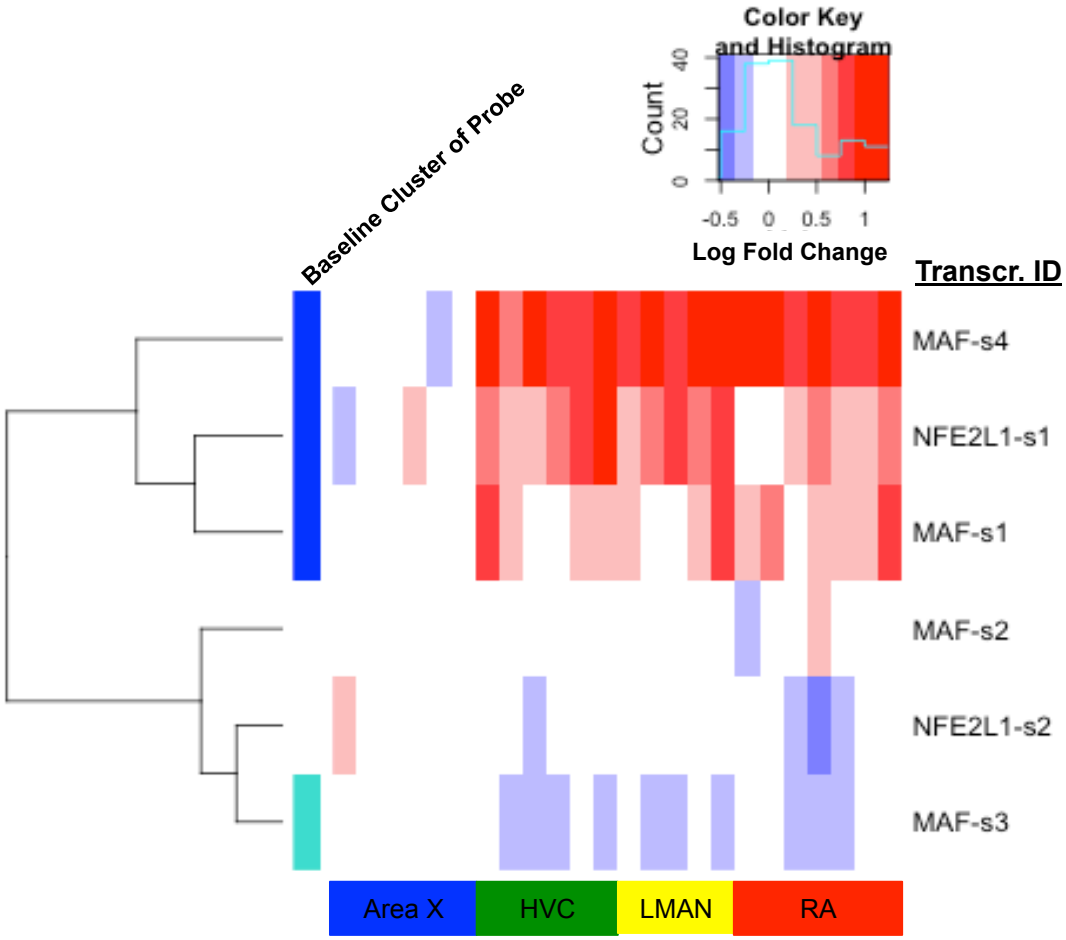

Supplementary Figure S6

A St WNT Ca2 Cyclic GMP Pathway

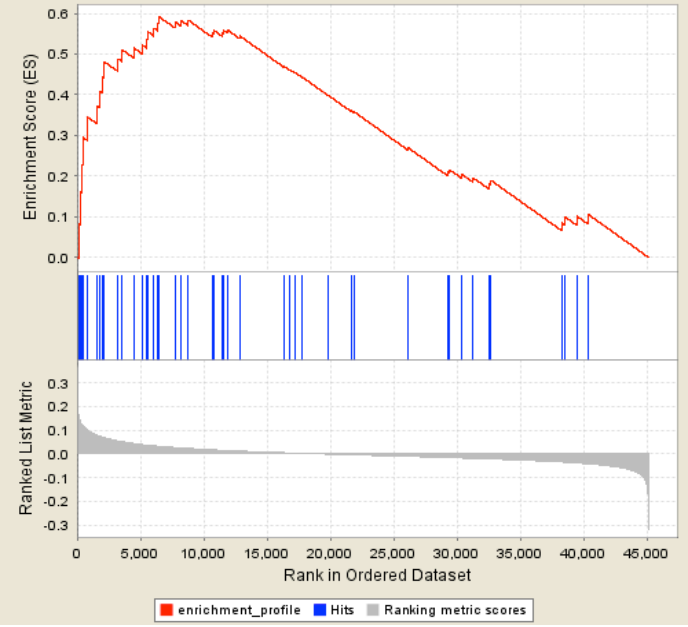

B GABA Pathway

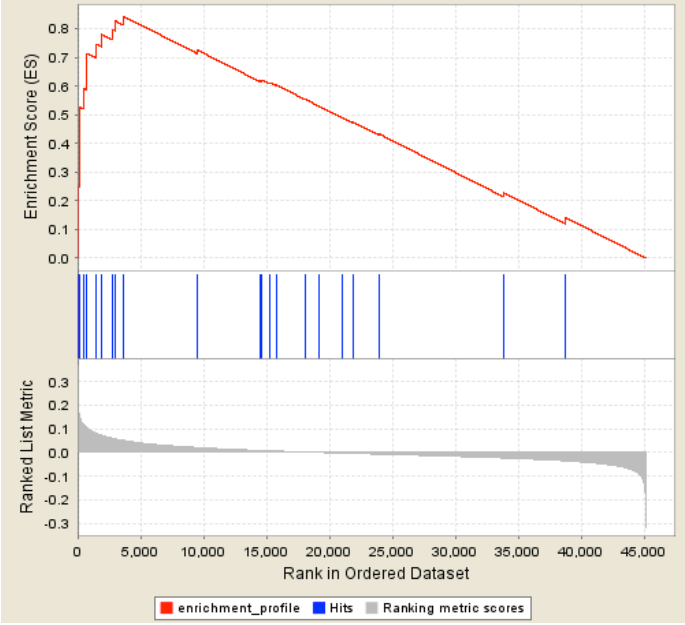

Supplementary Figure S7.

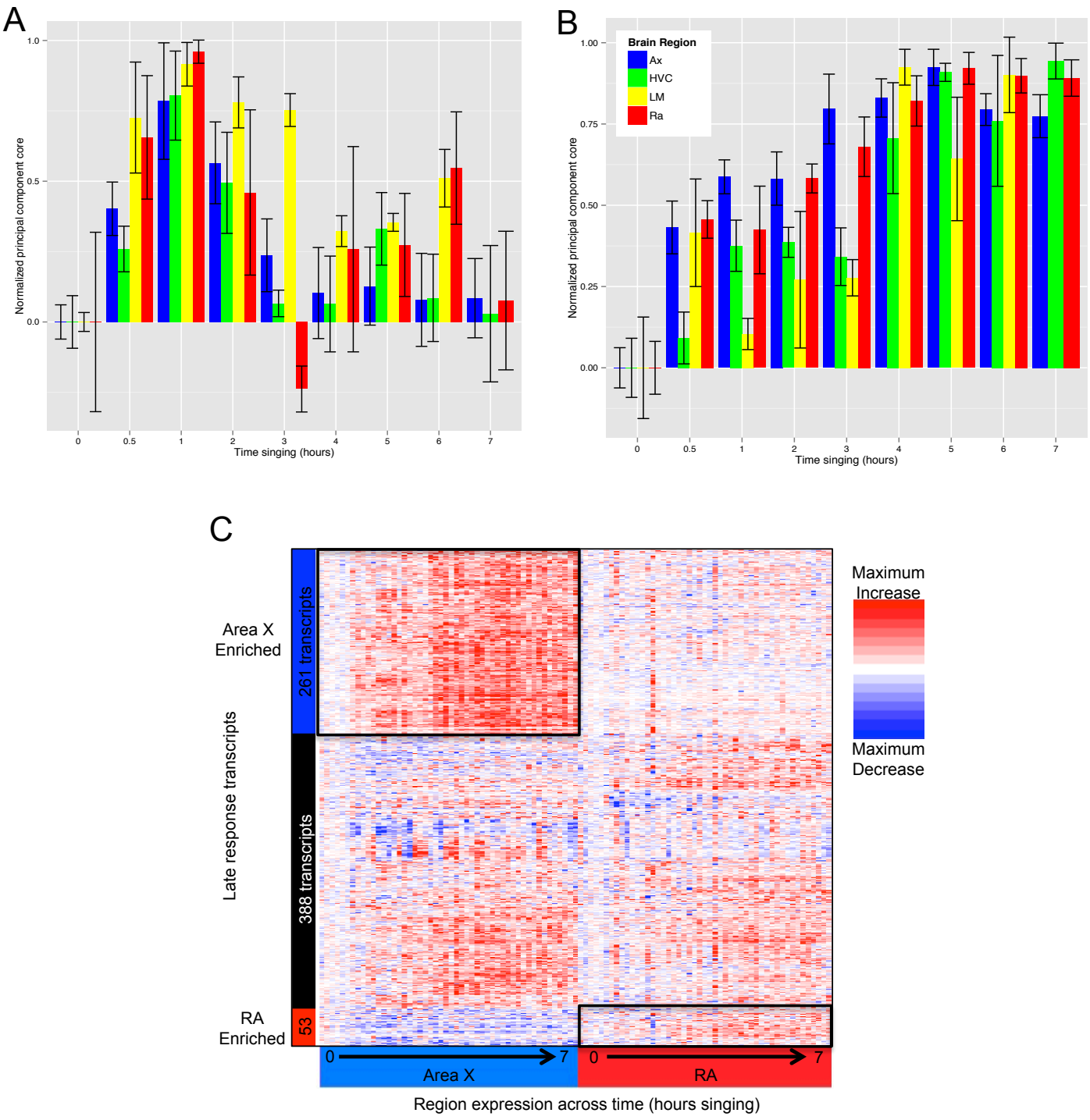

Supplementary Figure S8

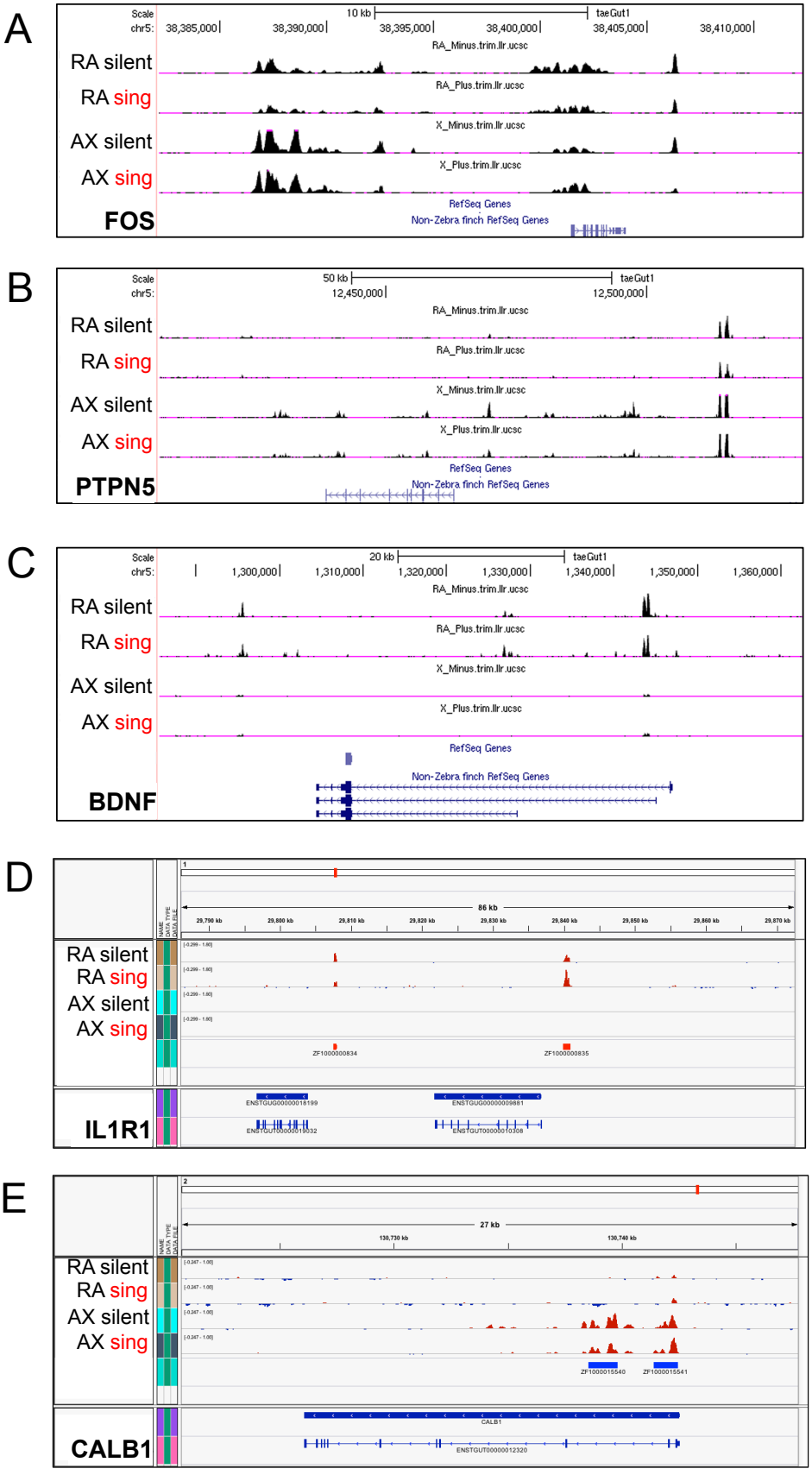

Supplementary Figure S9

A **Category of IEG-region enriched expression vs. baseline H3K27ac**

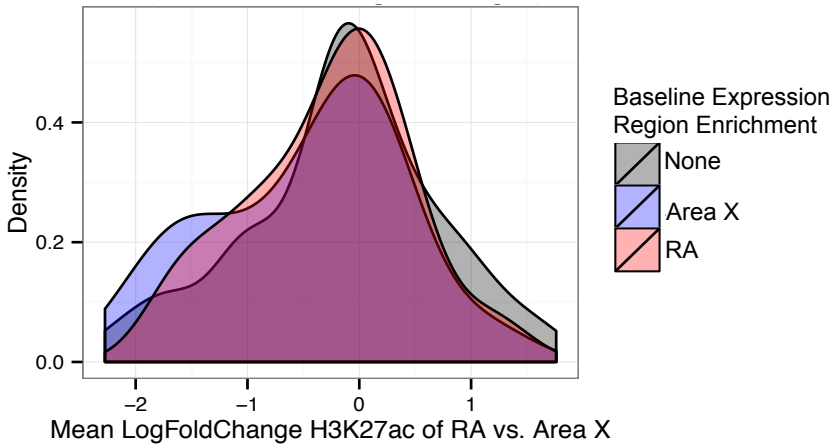

B **Category of late response gene decrease enriched expression vs. baseline H3K27ac**

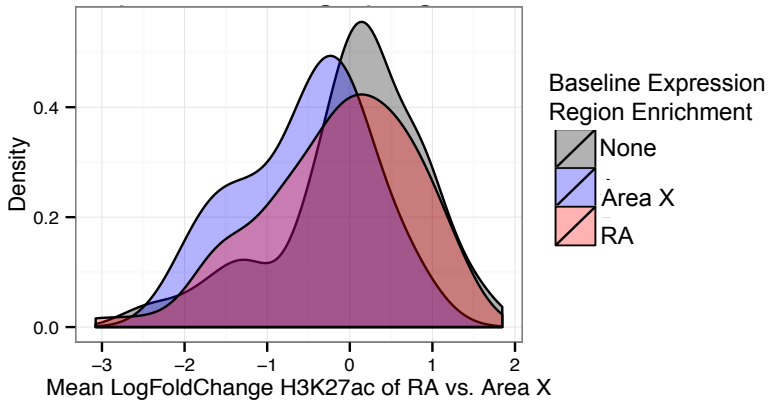

C **Comparing IEG gene induction to changes in H3K27ac during song production**

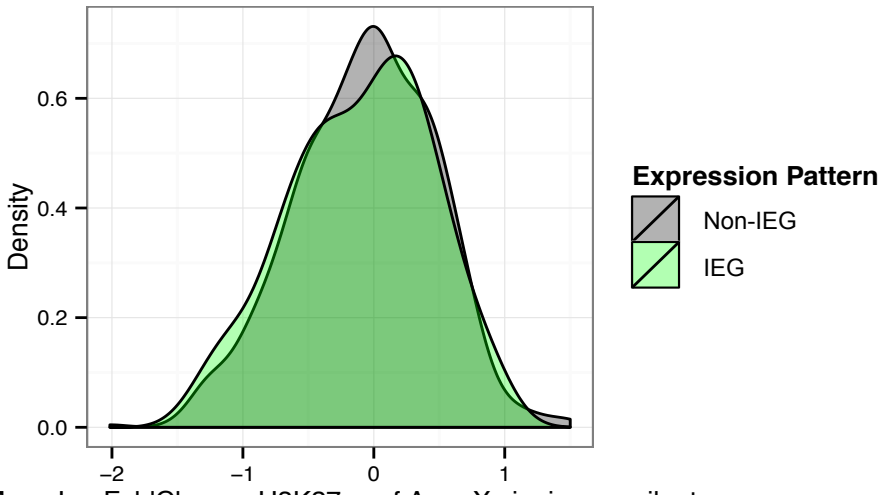

Supplementary Figure S10

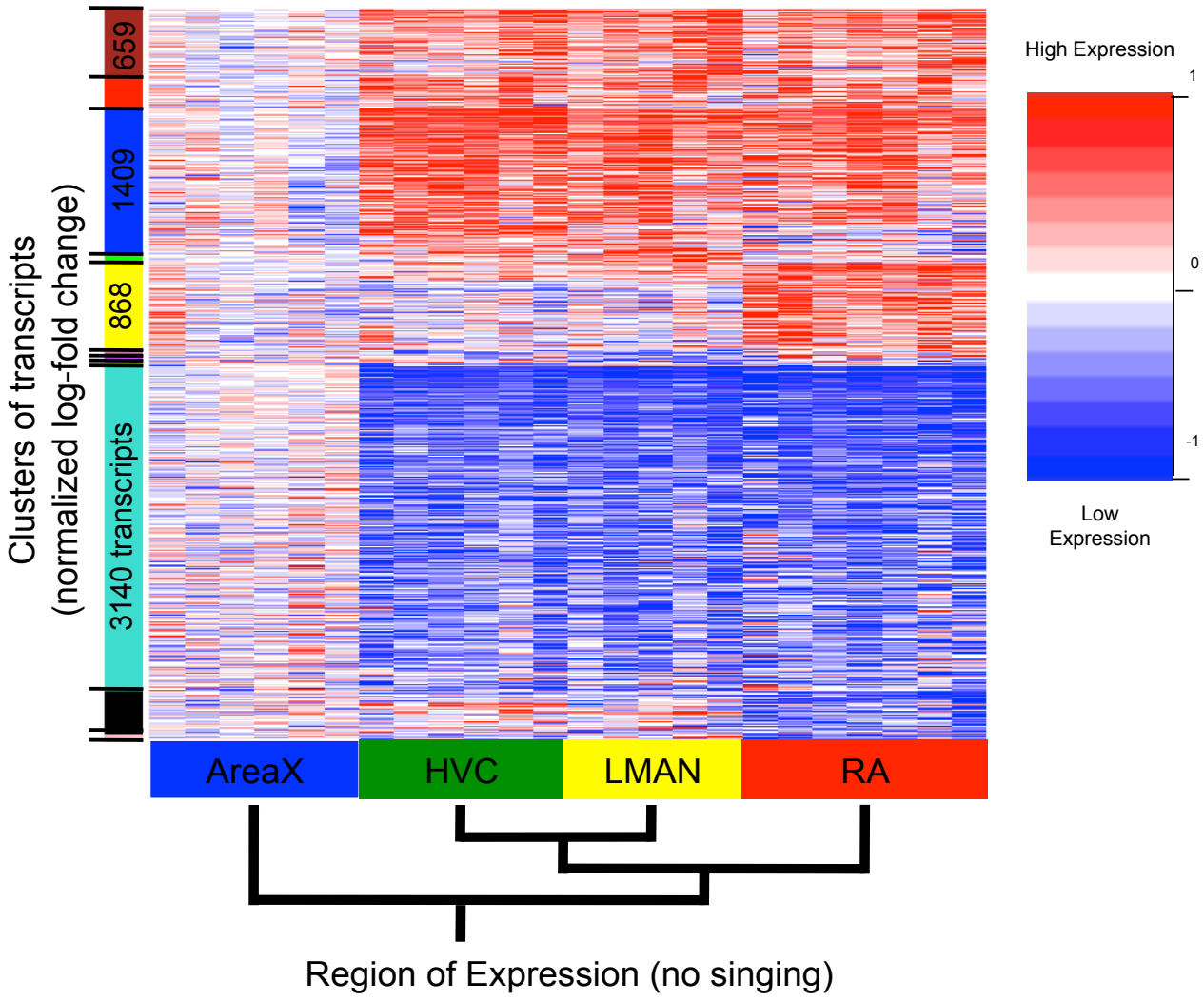

Supplementary Figure S11

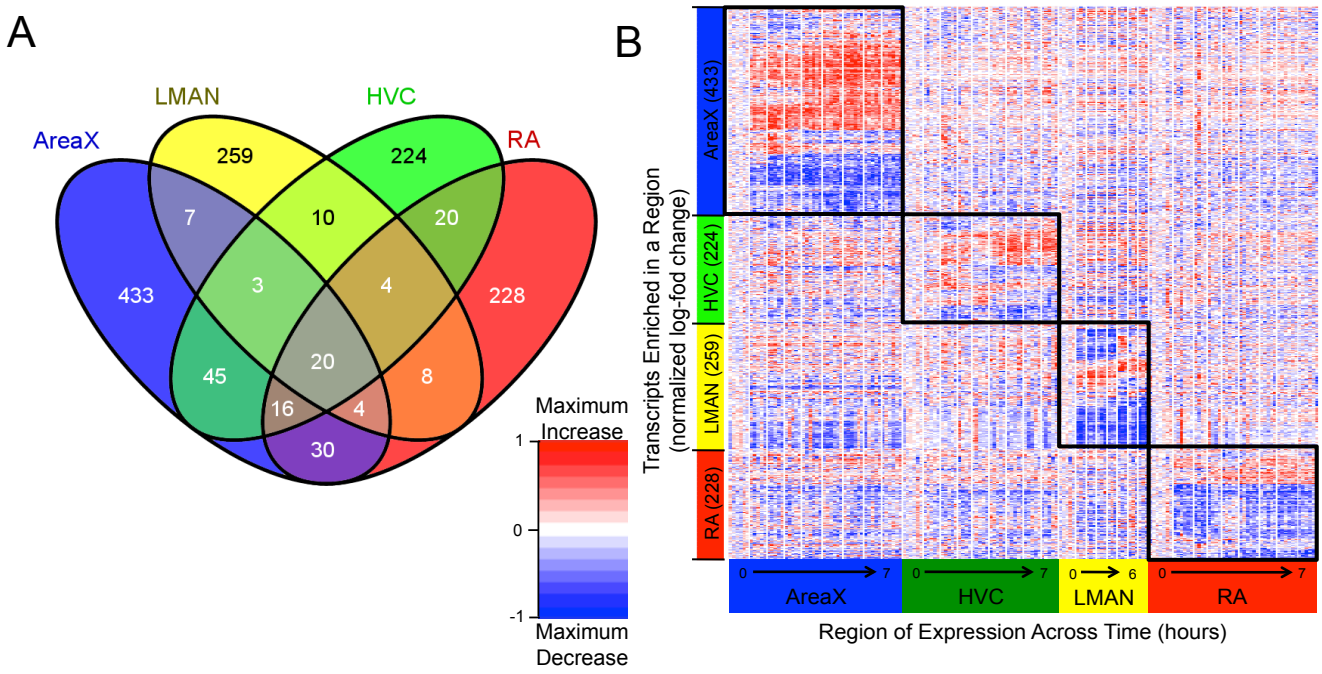

Supplementary Figure S12

References

1. A. J. Doupe, P. K. Kuhl, Birdsong and human speech: Common themes and mechanisms. *Annu. Rev. Neurosci.* **22**, 567–631 (1999). Medline doi:10.1146/annurev.neuro.22.1.567

2. E. D. Jarvis, Learned birdsong and the neurobiology of human language. *Ann. N. Y. Acad. Sci.* **1016**, 749–777 (2004). Medline doi:10.1196/annals.1298.038

3. R. Mooney, M. Konishi, Two distinct inputs to an avian song nucleus activate different glutamate receptor subtypes on individual neurons. *Proc. Natl. Acad. Sci. U.S.A.* **88**, 4075–4079 (1991). Medline doi:10.1073/pnas.88.10.4075

4. M. Luo, D. J. Perkel, A GABAergic, strongly inhibitory projection to a thalamic nucleus in the zebra finch song system. *J. Neurosci.* **19**, 6700–6711 (1999). Medline

5. A. Reiner, D. J. Perkel, L. L. Bruce, A. B. Butler, A. Csillag, W. Kuenzel, L. Medina, G. Paxinos, T. Shimizu, G. Striedter, M. Wild, G. F. Ball, S. Durand, O. Güntürkün, D. W. Lee, C. V. Mello, A. Powers, S. A. White, G. Hough, L. Kubikova, T. V. Smulders, K. Wada, J. Dugas-Ford, S. Husband, K. Yamamoto, J. Yu, C. Siang, E. D. Jarvis, O. Gütürkün; Avian Brain Nomenclature Forum, Revised nomenclature for avian telencephalon and some related brainstem nuclei. *J. Comp. Neurol.* **473**, 377–414 (2004). Medline doi:10.1002/cne.20118

6. E. D. Jarvis, O. Güntürkün, L. Bruce, A. Csillag, H. Karten, W. Kuenzel, L. Medina, G. Paxinos, D. J. Perkel, T. Shimizu, G. Striedter, J. M. Wild, G. F. Ball, J. Dugas-Ford, S. E. Durand, G. E. Hough, S. Husband, L. Kubikova, D. W. Lee, C. V. Mello, A. Powers, C. Siang, T. V. Smulders, K. Wada, S. A. White, K. Yamamoto, J. Yu, A. Reiner, A. B. Butler; Avian Brain Nomenclature Consortium, Avian brains and a new understanding of vertebrate brain evolution. *Nat. Rev. Neurosci.* **6**, 151–159 (2005). Medline doi:10.1038/nrn1606

7. F. Nottebohm, T. M. Stokes, C. M. Leonard, Central control of song in the canary, Serinus canarius. *J. Comp. Neurol.* **165**, 457–486 (1976). Medline doi:10.1002/cne.901650405

8. S. W. Bottjer, E. A. Miesner, A. P. Arnold, Forebrain lesions disrupt development but not maintenance of song in passerine birds. *Science* **224**, 901–903 (1984). Medline doi:10.1126/science.6719123

9. C. Scharff, F. Nottebohm, A comparative study of the behavioral deficits following lesions of various parts of the zebra finch song system: Implications for vocal learning. *J. Neurosci.* **11**, 2896–2913 (1991). Medline

10. H. Williams, N. Mehta, Changes in adult zebra finch song require a forebrain nucleus that is not necessary for song production. *J. Neurobiol.* **39**, 14–28 (1999). Medline doi:10.1002/(SICI)1097-4695(199904)39:1<14::AID-NEU2>3.0.CO;2-X

11. M. S. Brainard, A. J. Doupe, Interruption of a basal ganglia-forebrain circuit prevents plasticity of learned vocalizations. *Nature* **404**, 762–766 (2000). Medline doi:10.1038/35008083

12. B. P. Olveczky, A. S. Andalman, M. S. Fee, Vocal experimentation in the juvenile songbird requires a basal ganglia circuit. *PLOS Biol.* **3**, e153 (2005). Medline doi:10.1371/journal.pbio.0030153

13. D. Aronov, A. S. Andalman, M. S. Fee, A specialized forebrain circuit for vocal babbling in the juvenile songbird. *Science* **320**, 630–634 (2008). Medline doi:10.1126/science.1155140

14. S. W. Bottjer, F. Johnson, Circuits, hormones, and learning: Vocal behavior in songbirds. *J. Neurobiol.* **33**, 602–618 (1997). Medline doi:10.1002/(SICI)1097-4695(19971105)33:5<602::AID-NEU8>3.0.CO;2-8

15. A. R. Pfenning, E. Hara, O. Whitney, M. R. Rivas, P. Roulhac, J. T. Howard, M. Wirthlin, P. V. Lovell, G. Ganapathy, M. A. Moseley, J. W. Thompson, E. J. Soderblom, C. V. Mello, A. J. Hartemink, E. D. Jarvis, Convergent transcriptional specializations in the brains of humans and song learning birds. *Science* **346**, 1256846 (2014); doi:10.1126/science.1256846

16. C. Scharff, J. Petri, Evo-devo, deep homology and FoxP2: Implications for the evolution of speech and language. *Philos. Trans. R. Soc. Lond. B Biol. Sci.* **366**, 2124–2140 (2011). Medline doi:10.1098/rstb.2011.0001

17. E. D. Jarvis, F. Nottebohm, Motor-driven gene expression. *Proc. Natl. Acad. Sci. U.S.A.* **94**, 4097–4102 (1997). Medline doi:10.1073/pnas.94.8.4097

18. R. R. Kimpo, A. J. Doupe, FOS is induced by singing in distinct neuronal populations in a motor network. *Neuron* **18**, 315–325 (1997). Medline doi:10.1016/S0896-6273(00)80271-8

19. H. Jin, D. F. Clayton, Localized changes in immediate-early gene regulation during sensory and motor learning in zebra finches. *Neuron* **19**, 1049–1059 (1997). Medline doi:10.1016/S0896-6273(00)80396-7

20. E. D. Jarvis, C. Scharff, M. R. Grossman, J. A. Ramos, F. Nottebohm, For whom the bird sings: Context-dependent gene expression. *Neuron* **21**, 775–788 (1998). Medline doi:10.1016/S0896-6273(00)80594-2

21. O. Whitney, K. Soderstrom, F. Johnson, Post-transcriptional regulation of zenk expression associated with zebra finch vocal development. *Brain Res. Mol. Brain Res.* **80**, 279–290 (2000). Medline doi:10.1016/S0169-328X(00)00178-9

22. O. Whitney, F. Johnson, Motor-induced transcription but sensory-regulated translation of ZENK in socially interactive songbirds. *J. Neurobiol.* **65**, 251–259 (2005). Medline doi:10.1002/neu.20187

23. L. Kubikova, E. A. Turner, E. D. Jarvis, The pallial basal ganglia pathway modulates the behaviorally driven gene expression of the motor pathway. *Eur. J. Neurosci.* **25**, 2145–2160 (2007). Medline doi:10.1111/j.1460-9568.2007.05368.x

24. K. Wada, J. T. Howard, P. McConnell, O. Whitney, T. Lints, M. V. Rivas, H. Horita, M. A. Patterson, S. A. White, C. Scharff, S. Haesler, S. Zhao, H. Sakaguchi, M. Hagiwara, T. Shiraki, T. Hirozane-Kishikawa, P. Skene, Y. Hayashizaki, P. Carninci, E. D. Jarvis, A molecular neuroethological approach for identifying and characterizing a cascade of behaviorally regulated genes. *Proc. Natl. Acad. Sci. U.S.A.* **103**, 15212–15217 (2006). Medline doi:10.1073/pnas.0607098103

25. X. C. Li, E. D. Jarvis, B. Alvarez-Borda, D. A. Lim, F. Nottebohm, A relationship between behavior, neurotrophin expression, and new neuron survival. *Proc. Natl. Acad. Sci. U.S.A.* **97**, 8584–8589 (2000). Medline doi:10.1073/pnas.140222497

26. A. J. Lombardino, X.-C. Li, M. Hertel, F. Nottebohm, Replaceable neurons and neurodegenerative disease share depressed UCHL1 levels. *Proc. Natl. Acad. Sci. U.S.A.* **102**, 8036–8041 (2005). Medline doi:10.1073/pnas.0503239102

27. I. Teramitsu, S. A. White, FoxP2 regulation during undirected singing in adult songbirds. *J. Neurosci.* **26**, 7390–7394 (2006). Medline doi:10.1523/JNEUROSCI.1662-06.2006

28. J. E. Miller, E. Spiteri, M. C. Condro, R. T. Dosumu-Johnson, D. H. Geschwind, S. A. White, Birdsong decreases protein levels of FoxP2, a molecule required for human speech. *J. Neurophysiol.* **100**, 2015–2025 (2008). Medline doi:10.1152/jn.90415.2008

29. W. C. Warren, D. F. Clayton, H. Ellegren, A. P. Arnold, L. W. Hillier, A. Künstner, S. Searle, S. White, A. J. Vilella, S. Fairley, A. Heger, L. Kong, C. P. Ponting, E. D. Jarvis, C. V. Mello, P. Minx, P. Lovell, T. A. F. Velho, M. Ferris, C. N. Balakrishnan, S. Sinha, C. Blatti, S. E. London, Y. Li, Y.-C. Lin, J. George, J. Sweedler, B. Southey, P. Gunaratne, M. Watson, K. Nam, N. Backström, L. Smeds, B. Nabholz, Y. Itoh, O. Whitney, A. R. Pfenning, J. Howard, M. Völker, B. M. Skinner, D. K. Griffin, L. Ye, W. M. McLaren, P. Flicek, V. Quesada, G. Velasco, C. Lopez-Otin, X. S. Puente, T. Olender, D. Lancet, A. F. A. Smit, R. Hubley, M. K. Konkel, J. A. Walker, M. A. Batzer, W. Gu, D. D. Pollock, L. Chen, Z. Cheng, E. E. Eichler, J. Stapley, J. Slate, R. Ekblom, T. Birkhead, T. Burke, D. Burt, C. Scharff, I. Adam, H. Richard, M. Sultan, A. Soldatov, H. Lehrach, S. V. Edwards, S.-P. Yang, X. Li, T. Graves, L. Fulton, J. Nelson, A. Chinwalla, S. Hou, E. R. Mardis, R. K. Wilson, The genome of a songbird. *Nature* **464**, 757–762 (2010). Medline doi:10.1038/nature08819

30. A. T. Hilliard, J. E. Miller, E. R. Fraley, S. Horvath, S. A. White, Molecular microcircuitry underlies functional specification in a basal ganglia circuit dedicated to vocal learning. *Neuron* **73**, 537–552 (2012). Medline doi:10.1016/j.neuron.2012.01.005

31. G. Zhang *et al.*, Comparative genomics reveals insights into avian genome evolution and adaptation. *Science* **346**, 1311–1319 (2014); doi:10.1126/science.1251385

32. S. Haesler, K. Wada, A. Nshdejan, E. E. Morrisey, T. Lints, E. D. Jarvis, C. Scharff, FoxP2 expression in avian vocal learners and non-learners. *J. Neurosci.* **24**, 3164–3175 (2004). Medline doi:10.1523/JNEUROSCI.4369-03.2004

33. K. Wada, H. Sakaguchi, E. D. Jarvis, M. Hagiwara, Differential expression of glutamate receptors in avian neural pathways for learned vocalization. *J. Comp. Neurol.* **476**, 44–64 (2004). Medline doi:10.1002/cne.20201

34. L. Kubikova, K. Wada, E. D. Jarvis, Dopamine receptors in a songbird brain. *J. Comp. Neurol.* **518**, 741–769 (2010). Medline doi:10.1002/cne.22255

35. X. Li, X.-J. Wang, J. Tannenhauser, S. Podell, P. Mukherjee, M. Hertel, J. Biane, S. Masuda, F. Nottebohm, T. Gaasterland, Genomic resources for songbird research and their use in characterizing gene expression during brain development. *Proc. Natl. Acad. Sci. U.S.A.* **104**, 6834–6839 (2007). Medline doi:10.1073/pnas.0701619104

36. P. V. Lovell, D. F. Clayton, K. L. Replogle, C. V. Mello, Birdsong “transcriptomics”: Neurochemical specializations of the oscine song system. *PLOS ONE* **3**, e3440 (2008). Medline doi:10.1371/journal.pone.0003440

37. E. D. Jarvis, J. Yu, M. V. Rivas, H. Horita, G. Feenders, O. Whitney, S. C. Jarvis, E. R. Jarvis, L. Kubikova, A. E. Puck, C. Siang-Bakshi, S. Martin, M. McElroy, E. Hara, J. Howard, A. Pfenning, H. Mouritsen, C. C. Chen, K. Wada, Global view of the functional molecular organization of the avian cerebrum: Mirror images and functional columns. *J. Comp. Neurol.* **521**, 3614–3665 (2013). Medline doi:10.1002/cne.23404

38. M. R. Lyons, A. E. West, Mechanisms of specificity in neuronal activity-regulated gene transcription. *Prog. Neurobiol.* **94**, 259–295 (2011). Medline doi:10.1016/j.pneurobio.2011.05.003

39. S. W. Flavell, T.-K. Kim, J. M. Gray, D. A. Harmin, M. Hemberg, E. J. Hong, E. Markenscoff-Papadimitriou, D. M. Bear, M. E. Greenberg, Genome-wide analysis of MEF2 transcriptional program reveals synaptic target genes and neuronal activity-dependent polyadenylation site selection. *Neuron* **60**, 1022–1038 (2008). Medline doi:10.1016/j.neuron.2008.11.029

40. T.-K. Kim, M. Hemberg, J. M. Gray, A. M. Costa, D. M. Bear, J. Wu, D. A. Harmin, M. Laptewicz, K. Barbara-Haley, S. Kuersten, E. Markenscoff-Papadimitriou, D. Kuhl, H. Bito, P. F. Worley, G. Kreiman, M. E. Greenberg, Widespread transcription at neuronal activity-regulated enhancers. *Nature* **465**, 182–187 (2010). Medline doi:10.1038/nature09033

41. S. Dong, K. L. Replogle, L. Hasadsri, B. S. Imai, P. M. Yau, S. Rodriguez-Zas, B. R. Southey, J. V. Sweedler, D. F. Clayton, Discrete molecular states in the brain accompany changing responses to a vocal signal. *Proc. Natl. Acad. Sci. U.S.A.* **106**, 11364–11369 (2009). Medline doi:10.1073/pnas.0812998106

42. G. Feenders, M. Liedvogel, M. Rivas, M. Zapka, H. Horita, E. Hara, K. Wada, H. Mouritsen, E. D. Jarvis, Molecular mapping of movement-associated areas in the avian brain: A motor theory for vocal learning origin. *PLOS ONE* **3**, e1768 (2008). Medline doi:10.1371/journal.pone.0001768

43. C. S. Hill, R. Treisman, Growth factors and gene expression: Fresh insights from arrays. *Sci. STKE* **1999**, PE1 (1999). Medline doi:10.1126/stke.1999.3.pe1

44. A. Barco, J. M. Alarcon, E. R. Kandel, Expression of constitutively active CREB protein facilitates the late phase of long-term potentiation by enhancing synaptic capture. *Cell* **108**, 689–703 (2002). Medline doi:10.1016/S0092-8674(02)00657-8

45. S. Sinha, On counting position weight matrix matches in a sequence, with application to discriminative motif finding. *Bioinformatics* **22**, e454–e463 (2006). Medline doi:10.1093/bioinformatics/btl227

46. J. Kim, R. Cunningham, B. James, S. Wyder, J. D. Gibson, O. Niehuis, E. M. Zdobnov, H. M. Robertson, G. E. Robinson, J. H. Werren, S. Sinha, Functional characterization of transcription factor motifs using cross-species comparison across large evolutionary distances. *PLOS Comput. Biol.* **6**, e1000652 (2010). Medline doi:10.1371/journal.pcbi.1000652

47. A. R. Pfenning, R. Schwartz, A. L. Barth, A comparative genomics approach to identifying the plasticity transcriptome. *BMC Neurosci.* **8**, 20 (2007). Medline doi:10.1186/1471-2202-8-20

48. A. R. Pfenning, T.-K. Kim, J. M. Spotts, M. Hemberg, D. Su, A. E. West, Genome-wide identification of calcium-response factor (CaRF) binding sites predicts a role in regulation of neuronal signaling pathways. *PLOS ONE* **5**, e10870 (2010). Medline doi:10.1371/journal.pone.0010870

49. S. W. Flavell, M. E. Greenberg, Signaling mechanisms linking neuronal activity to gene expression and plasticity of the nervous system. *Annu. Rev. Neurosci.* **31**, 563–590 (2008). Medline doi:10.1146/annurev.neuro.31.060407.125631

50. S. Loebrich, E. Nedivi, The function of activity-regulated genes in the nervous system. *Physiol. Rev.* **89**, 1079–1103 (2009). Medline doi:10.1152/physrev.00013.2009

51. X. Cao, R. Mahendran, G. R. Guy, Y. H. Tan, Detection and characterization of cellular EGR-1 binding to its recognition site. *J. Biol. Chem.* **268**, 16949–16957 (1993). Medline

52. O. Johnsen, N. Skammelsrud, L. Luna, M. Nishizawa, H. Prydz, A. B. A. Kolstø, Small Maf proteins interact with the human transcription factor TCF11/Nrf1/LCR-F1. *Nucleic Acids Res.* **24**, 4289–4297 (1996). Medline doi:10.1093/nar/24.21.4289

53. A. Subramanian, P. Tamayo, V. K. Mootha, S. Mukherjee, B. L. Ebert, M. A. Gillette, A. Paulovich, S. L. Pomeroy, T. R. Golub, E. S. Lander, J. P. Mesirov, Gene set enrichment analysis: A knowledge-based approach for interpreting genome-wide expression profiles. *Proc. Natl. Acad. Sci. U.S.A.* **102**, 15545–15550 (2005). Medline doi:10.1073/pnas.0506580102

54. K. A. McDowell, A. N. Hutchinson, S. J. E. Wong-Goodrich, M. M. Presby, D. Su, R. M. Rodriguiz, K. C. Law, C. L. Williams, W. C. Wetsel, A. E. West, Reduced cortical BDNF expression and aberrant memory in Carf knock-out mice. *J. Neurosci.* **30**, 7453–7465 (2010). Medline doi:10.1523/JNEUROSCI.3997-09.2010

55.ENCODE Project Consortium, An integrated encyclopedia of DNA elements in the human genome. *Nature* **489**, 57–74 (2012). Medline doi:10.1038/nature11247

56. UCSC Genome Browser; https://genome.ucsc.edu/cgi-bin/hgTracks?hgS_doOtherUser=submit&hgS_otherUserName=apfenning&hgS_otherUserSessionName=taeGut1_basic (2014).

57. P. Goelet, V. F. Castellucci, S. Schacher, E. R. Kandel, The long and the short of long-term memory—A molecular framework. *Nature* **322**, 419–422 (1986). Medline doi:10.1038/322419a0

58. A. N. Malik, T. Vierbuchen, M. Hemberg, A. A. Rubin, E. Ling, C. H. Couch, H. Stroud, I. Spiegel, K. K. Farh, D. A. Harmin, M. E. Greenberg, Genome-wide identification and characterization of functional neuronal activity-dependent enhancers. *Nat. Neurosci.* **17**, 1330–1339 (2014). Medline doi:10.1038/nn.3808

59. A. E. West, M. E. Greenberg, Neuronal activity-regulated gene transcription in synapse development and cognitive function. *Cold Spring Harb. Perspect. Biol.* **3**, a005744–a005744 (2011). Medline doi:10.1101/cshperspect.a005744

60. I. Spiegel, A. R. Mardinly, H. W. Gabel, J. E. Bazinet, C. H. Couch, C. P. Tzeng, D. A. Harmin, M. E. Greenberg, Npas4 regulates excitatory-inhibitory balance within neural circuits through cell-type-specific gene programs. *Cell* **157**, 1216–1229 (2014). Medline doi:10.1016/j.cell.2014.03.058

61. H. Horita, K. Wada, M. V. Rivas, E. Hara, E. D. Jarvis, The dusp1 immediate early gene is regulated by natural stimuli predominantly in sensory input neurons. *J. Comp. Neurol.* **518**, 2873–2901 (2010). Medline

62. H. Horita, M. Kobayashi, W. C. Liu, K. Oka, E. D. Jarvis, K. Wada, Specialized motor-driven dusp1 expression in the song systems of multiple lineages of vocal learning birds. *PLOS ONE* **7**, e42173 (2012). Medline doi:10.1371/journal.pone.0042173

63. K. Sakamoto, K. Karelina, K. Obrietan, CREB: A multifaceted regulator of neuronal plasticity and protection. *J. Neurochem.* **116**, 1–9 (2011). Medline doi:10.1111/j.1471-4159.2010.07080.x

64. J. I. Morgan, T. Curran, Stimulus-transcription coupling in neurons: Role of cellular immediate-early genes. *Trends Neurosci.* **12**, 459–462 (1989). Medline doi:10.1016/0166-2236(89)90096-9

65. C. H. Bailey, D. Bartsch, E. R. Kandel, Toward a molecular definition of long-term memory storage. *Proc. Natl. Acad. Sci. U.S.A.* **93**, 13445–13452 (1996). Medline doi:10.1073/pnas.93.24.13445

66. J. M. Wettenhall, G. K. Smyth, limmaGUI: A graphical user interface for linear modeling of microarray data. *Bioinformatics* **20**, 3705–3706 (2004). Medline doi:10.1093/bioinformatics/bth449

67. P. L. Roulhac, J. M. Ward, J. W. Thompson, E. J. Soderblom, M. Silva, M. A. Moseley 3rd, E. D. Jarvis, Microproteomics: Quantitative proteomic profiling of small numbers of laser-captured cells. *Cold Spring Harbor Protocols* **2011**, 218–234 (2011). Medline doi:10.1101/pdb.prot5573

68. K. Replogle, A. P. Arnold, G. F. Ball, M. Band, S. Bensch, E. A. Brenowitz, S. Dong, J. Drnevich, M. Ferris, J. M. George, G. Gong, D. Hasselquist, A. G. Hernandez, R. Kim, H. A. Lewin, L. Liu, P. V. Lovell, C. V. Mello, S. Naurin, S. Rodriguez-Zas, J. Thimmapuram, J. Wade, D. F. Clayton, The Songbird Neurogenomics, The Songbird Neurogenomics (SoNG) Initiative: Community-based tools and strategies for study of brain gene function and evolution. *BMC Genomics* **9**, 131 (2008). Medline doi:10.1186/1471-2164-9-131

69. B. J. Haas, S. L. Salzberg, W. Zhu, M. Pertea, J. E. Allen, J. Orvis, O. White, C. R. Buell, J. R. Wortman, Automated eukaryotic gene structure annotation using EVidenceModeler and the Program to Assemble Spliced Alignments. *Genome Biol.* **9**, R7 (2008). Medline doi:10.1186/gb-2008-9-1-r7

70. P. Flicek, M. R. Amode, D. Barrell, K. Beal, S. Brent, Y. Chen, P. Clapham, G. Coates, S. Fairley, S. Fitzgerald, L. Gordon, M. Hendrix, T. Hourlier, N. Johnson, A. Kähäri, D. Keefe, S. Keenan, R. Kinsella, F. Kokocinski, E. Kulesha, P. Larsson, I. Longden, W. McLaren, B. Overduin, B. Pritchard, H. S. Riat, D. Rios, G. R. S. Ritchie, M. Ruffier, M. Schuster, D. Sobral, G. Spudich, Y. A. Tang, S. Trevanion, J. Vandrovcova, A. J. Vilella, S. White, S. P. Wilder, A. Zadissa, J. Zamora, B. L. Aken, E. Birney, F. Cunningham, I.

Dunham, R. Durbin, X. M. Fernández-Suarez, J. Herrero, T. J. P. Hubbard, A. Parker, G. Proctor, J. Vogel, S. M. J. Searle, Ensembl 2011. *Nucleic Acids Res.* **39** (Database), D800–D806 (2011). Medline doi:10.1093/nar/gkq1064

71. A. R. Quinlan, I. M. Hall, BEDTools: A flexible suite of utilities for comparing genomic features. *Bioinformatics* **26**, 841–842 (2010). Medline doi:10.1093/bioinformatics/btq033

72. K. D. Pruitt, T. Tatusova, D. R. Maglott, NCBI reference sequences (RefSeq): A curated non-redundant sequence database of genomes, transcripts and proteins. *Nucleic Acids Res.* **35** (Database), D61–D65 (2007). Medline doi:10.1093/nar/gkl842

73. D. A. Benson, I. Karsch-Mizrachi, D. J. Lipman, J. Ostell, E. W. Sayers, GenBank. *Nucleic Acids Res.* **37** (Database), D26–D31 (2009). Medline doi:10.1093/nar/gkn723

74. R. C. Gentleman, V. J. Carey, D. M. Bates, B. Bolstad, M. Dettling, S. Dudoit, B. Ellis, L. Gautier, Y. Ge, J. Gentry, K. Hornik, T. Hothorn, W. Huber, S. Iacus, R. Irizarry, F. Leisch, C. Li, M. Maechler, A. J. Rossini, G. Sawitzki, C. Smith, G. Smyth, L. Tierney, J. Y. H. Yang, J. Zhang, Bioconductor: Open software development for computational biology and bioinformatics. *Genome Biol.* **5**, R80 (2004). Medline doi:10.1186/gb-2004-5-10-r80

75. W. Stacklies, H. Redestig, M. Scholz, D. Walther, J. Selbig, pcaMethods—a bioconductor package providing PCA methods for incomplete data. *Bioinformatics* **23**, 1164–1167 (2007). Medline doi:10.1093/bioinformatics/btm069

76. W. Huber, A. von Heydebreck, H. Sültmann, A. Poustka, M. Vingron, Variance stabilization applied to microarray data calibration and to the quantification of differential expression. *Bioinformatics* **18** (Suppl 1), S96–S104 (2002). Medline doi:10.1093/bioinformatics/18.suppl_1.S96

77. J. M. George, H. Jin, W. S. Woods, D. F. Clayton, Characterization of a novel protein regulated during the critical period for song learning in the zebra finch. *Neuron* **15**, 361–372 (1995). Medline doi:10.1016/0896-6273(95)90040-3

78. J. H. Ward Jr., Hierarchical Grouping to Optimize an Objective Function. *J. Am. Stat. Assoc.* **58**, 236–244 (1963). doi:10.1080/01621459.1963.10500845

79. K. S. Pollard, S. Dudoit, M. J. Van Der Laan, Multiple testing procedures: R multtest package and applications to genomics. http://biostats.bepress.com/ucbbiostat/paper164/, (2004).

80. A. S. Adler, S. Sinha, T. L. A. Kawahara, J. Y. Zhang, E. Segal, H. Y. Chang, Motif module map reveals enforcement of aging by continual NF-kappaB activity. *Genes Dev.* **21**, 3244–3257 (2007). Medline doi:10.1101/gad.1588507

81. S. Sinha, A. S. Adler, Y. Field, H. Y. Chang, E. Segal, Systematic functional characterization of cis-regulatory motifs in human core promoters. *Genome Res.* **18**, 477–488 (2008). Medline doi:10.1101/gr.6828808

82. C. Alaux, S. Sinha, L. Hasadsri, G. J. Hunt, E. Guzmán-Novoa, G. DeGrandi-Hoffman, J. L. Uribe-Rubio, B. R. Southey, S. Rodriguez-Zas, G. E. Robinson, Honey bee aggression supports a link between gene regulation and behavioral evolution. *Proc. Natl. Acad. Sci. U.S.A.* **106**, 15400–15405 (2009). Medline doi:10.1073/pnas.0907043106

83. S. Sinha, X. Ling, C. W. Whitfield, C. Zhai, G. E. Robinson, Genome scan for cis-regulatory DNA motifs associated with social behavior in honey bees. *Proc. Natl. Acad. Sci. U.S.A.* **103**, 16352–16357 (2006). Medline doi:10.1073/pnas.0607448103

84. J. C. Bryne, E. Valen, M.-H. E. Tang, T. Marstrand, O. Winther, I. da Piedade, A. Krogh, B. Lenhard, A. Sandelin, JASPAR, the open access database of transcription factor-binding profiles: New content and tools in the 2008 update. *Nucleic Acids Res.* **36** (Database), D102–D106 (2008). Medline doi:10.1093/nar/gkm955

85. E. Wingender, The TRANSFAC project as an example of framework technology that supports the analysis of genomic regulation. *Brief. Bioinform.* **9**, 326–332 (2008). Medline doi:10.1093/bib/bbn016

86. J. D. Storey, R. Tibshirani, Statistical significance for genomewide studies. *Proc. Natl. Acad. Sci. U.S.A.* **100**, 9440–9445 (2003). Medline doi:10.1073/pnas.1530509100

87. M. Kazemian, Q. Zhu, M. S. Halfon, S. Sinha, Improved accuracy of supervised CRM discovery with interpolated Markov models and cross-species comparison. *Nucleic Acids Res.* **39**, 9463–9472 (2011). Medline doi:10.1093/nar/gkr621

88. P. Zhou, M. Porcionatto, M. Pilapil, Y. Chen, Y. Choi, K. F. Tolias, J. B. Bikoff, E. J. Hong, M. E. Greenberg, R. A. Segal, Polarized signaling endosomes coordinate BDNF-induced chemotaxis of cerebellar precursors. *Neuron* **55**, 53–68 (2007). Medline doi:10.1016/j.neuron.2007.05.030

89. R. A. Irizarry, B. M. Bolstad, F. Collin, L. M. Cope, B. Hobbs, T. P. Speed, Summaries of Affymetrix GeneChip probe level data. *Nucleic Acids Res.* **31**, e15 (2003). Medline doi:10.1093/nar/gng015

90. T. Beissbarth, T. P. Speed, GOstat: Find statistically overrepresented Gene Ontologies within a group of genes. *Bioinformatics* **20**, 1464–1465 (2004). Medline doi:10.1093/bioinformatics/bth088

91. M. Hollander, D. A. Wolfe, *Nonparametric statistical methods*. (John Wiley and Sons, New York, ed. 2nd, 1999), pp. 787.

92. J. Michaud, K. M. Simpson, R. Escher, K. Buchet-Poyau, T. Beissbarth, C. Carmichael, M. E. Ritchie, F. Schütz, P. Cannon, M. Liu, X. Shen, Y. Ito, W. H. Raskind, M. S. Horwitz, M. Osato, D. R. Turner, T. P. Speed, M. Kavallaris, G. K. Smyth, H. S. Scott, Integrative analysis of RUNX1 downstream pathways and target genes. *BMC Genomics* **9**, 363 (2008). Medline doi:10.1186/1471-2164-9-363

93. H. Li, B. Handsaker, A. Wysoker, T. Fennell, J. Ruan, N. Homer, G. Marth, G. Abecasis, R. Durbin; 1000 Genome Project Data Processing Subgroup, The Sequence Alignment/Map format and SAMtools. *Bioinformatics* **25**, 2078–2079 (2009). Medline doi:10.1093/bioinformatics/btp352

94. T. Bailey, P. Krajewski, I. Ladunga, C. Lefebvre, Q. Li, T. Liu, P. Madrigal, C. Taslim, J. Zhang, Practical guidelines for the comprehensive analysis of ChIP-seq data. *PLOS Comput. Biol.* **9**, e1003326 (2013). Medline doi:10.1371/journal.pcbi.1003326

95. P. V. Kharchenko, M. Y. Tolstorukov, P. J. Park, Design and analysis of ChIP-seq experiments for DNA-binding proteins. *Nat. Biotechnol.* **26**, 1351–1359 (2008). Medline doi:10.1038/nbt.1508

96. A. T. Lun, G. K. Smyth, De novo detection of differentially bound regions for ChIP-seq data using peaks and windows: Controlling error rates correctly. *Nucleic Acids Res.* **42**, e95 (2014). Medline doi:10.1093/nar/gku351

97. Q. Li, J. B. Brown, H. Huang, P. J. Bickel, Measuring reproducibility of high-throughput experiments. *Ann. Appl. Stat.* **5**, 1752–1779 (2011). doi:10.1214/11-AOAS466

98. E. Birney, J. A. Stamatoyannopoulos, A. Dutta, R. Guigó, T. R. Gingeras, E. H. Margulies, Z. Weng, M. Snyder, E. T. Dermitzakis, R. E. Thurman, M. S. Kuehn, C. M. Taylor, S. Neph, C. M. Koch, S. Asthana, A. Malhotra, I. Adzhubei, J. A. Greenbaum, R. M. Andrews, P. Flicek, P. J. Boyle, H. Cao, N. P. Carter, G. K. Clelland, S. Davis, N. Day, P. Dhami, S. C. Dillon, M. O. Dorschner, H. Fiegler, P. G. Giresi, J. Goldy, M. Hawrylycz, A. Haydock, R. Humbert, K. D. James, B. E. Johnson, E. M. Johnson, T. T. Frum, E. R. Rosenzweig, N. Karnani, K. Lee, G. C. Lefebvre, P. A. Navas, F. Neri, S. C. Parker, P. J. Sabo, R. Sandstrom, A. Shafer, D. Vetrie, M. Weaver, S. Wilcox, M. Yu, F. S. Collins, J. Dekker, J. D. Lieb, T. D. Tullius, G. E. Crawford, S. Sunyaev, W. S. Noble, I. Dunham, F. Denoeud, A. Reymond, P. Kapranov, J. Rozowsky, D. Zheng, R. Castelo, A. Frankish, J. Harrow, S. Ghosh, A. Sandelin, I. L. Hofacker, R. Baertsch, D. Keefe, S. Dike, J. Cheng, H. A. Hirsch, E. A. Sekinger, J. Lagarde, J. F. Abril, A. Shahab, C. Flamm, C. Fried, J. Hackermüller, J. Hertel, M. Lindemeyer, K. Missal, A. Tanzer, S. Washietl, J. Korbel, O. Emanuelsson, J. S. Pedersen, N. Holroyd, R. Taylor, D. Swarbreck, N. Matthews, M. C. Dickson, D. J. Thomas, M. T. Weirauch, J. Gilbert, J. Drenkow, I. Bell, X. Zhao, K. G. Srinivasan, W. K. Sung, H. S. Ooi, K. P. Chiu, S. Foissac, T. Alioto, M. Brent, L. Pachter, M. L. Tress, A. Valencia, S. W. Choo, C. Y. Choo, C. Ucla, C. Manzano, C. Wyss, E. Cheung, T. G. Clark, J. B. Brown, M. Ganesh, S. Patel, H. Tammana, J. Chrast, C. N. Henrichsen, C. Kai, J. Kawai, U. Nagalakshmi, J. Wu, Z. Lian, J. Lian, P. Newburger, X. Zhang, P. Bickel, J. S. Mattick, P. Carninci, Y. Hayashizaki, S. Weissman, T. Hubbard, R. M. Myers, J. Rogers, P. F. Stadler, T. M. Lowe, C. L. Wei, Y. Ruan, K. Struhl, M. Gerstein, S. E. Antonarakis, Y. Fu, E. D. Green, U. Karaöz, A. Siepel, J. Taylor, L. A. Liefer, K. A. Wetterstrand, P. J. Good, E. A. Feingold, M. S. Guyer, G. M. Cooper, G. Asimenos, C. N. Dewey, M. Hou, S. Nikolaev, J. I. Montoya-Burgos, A. Löytynoja, S. Whelan, F. Pardi, T. Massingham, H. Huang, N. R. Zhang, I. Holmes, J. C. Mullikin, A. Ureta-Vidal, B. Paten, M. Seringhaus, D. Church, K. Rosenbloom, W. J. Kent, E. A. Stone, S. Batzoglou, N. Goldman, R. C. Hardison, D. Haussler, W. Miller, A. Sidow, N. D. Trinklein, Z. D. Zhang, L. Barrera, R. Stuart, D. C. King, A. Ameur, S. Enroth, M. C. Bieda, J. Kim, A. A. Bhinge, N. Jiang, J. Liu, F. Yao, V. B. Vega, C. W. Lee, P. Ng, A. Shahab, A. Yang, Z. Moqtaderi, Z. Zhu, X. Xu, S. Squazzo, M. J. Oberley, D. Inman, M. A. Singer, T. A. Richmond, K. J. Munn, A. Rada-Iglesias, O. Wallerman, J. Komorowski, J. C. Fowler, P. Couttet, A. W. Bruce, O. M. Dovey, P. D. Ellis, C. F. Langford, D. A. Nix, G. Euskirchen, S. Hartman, A. E. Urban, P. Kraus, S. Van Calcar, N. Heintzman, T. H. Kim, K. Wang, C. Qu, G. Hon, R. Luna, C. K. Glass, M. G. Rosenfeld, S. F. Aldred, S. J. Cooper, A. Halees, J. M. Lin, H. P. Shulha, X. Zhang, M. Xu, J. N. Haidar, Y. Yu, Y. Ruan, V. R. Iyer, R. D. Green, C. Wadelius, P. J. Farnham, B. Ren, R. A. Harte, A. S. Hinrichs, H. Trumbower, H. Clawson, J. Hillman-Jackson, A. S. Zweig, K. Smith, A. Thakkapallayil, G. Barber, R. M. Kuhn, D. Karolchik, L. Armengol, C. P. Bird, P. I. de Bakker, A. D. Kern, N. Lopez-Bigas, J. D. Martin, B. E. Stranger, A. Woodroffe, E. Davydov, A. Dimas, E. Eyras, I. B. Hallgrímsdóttir, J. Huppert, M. C. Zody, G. R. Abecasis, X. Estivill, G. G. Bouffard, X. Guan, N. F. Hansen, J. R. Idol, V. V. Maduro, B. Maskeri, J. C. McDowell, M. Park, P. J.

Thomas, A. C. Young, R. W. Blakesley, D. M. Muzny, E. Sodergren, D. A. Wheeler, K. C. Worley, H. Jiang, G. M. Weinstock, R. A. Gibbs, T. Graves, R. Fulton, E. R. Mardis, R. K. Wilson, M. Clamp, J. Cuff, S. Gnerre, D. B. Jaffe, J. L. Chang, K. Lindblad-Toh, E. S. Lander, M. Koriabine, M. Nefedov, K. Osoegawa, Y. Yoshinaga, B. Zhu, P. J. de Jong; ENCODE Project Consortium, Identification and analysis of functional elements in 1% of the human genome by the ENCODE pilot project. *Nature* **447**, 799–816 (2007). Medline doi:10.1038/nature05874

99. M. Love, W. Hunber, S. Anders, Moderated estimation of fold change and dispersion for RNA-seq data with DESeq2. *bioRxiv* 10.1101/002832 (2014); http://dx.doi.org/10.1101/002832

100. J. M. Wettenhall, G. K. Smyth, limmaGUI: A graphical user interface for linear modeling of microarray data. *Bioinformatics* **20**, 3705–3706 (2004). Medline doi:10.1093/bioinformatics/bth449

101. E. Garcia-Calero, C. Scharff, Calbindin expression in developing striatum of zebra finches and its relation to the formation of area X. *J. Comp. Neurol.* **521**, 326–341 (2013). Medline doi:10.1002/cne.23174

102. T. A. F. Velho, P. Lovell, C. V. Mello, Enriched expression and developmental regulation of the middle-weight neurofilament (NF-M) gene in song control nuclei of the zebra finch. *J. Comp. Neurol.* **500**, 477–497 (2007). Medline doi:10.1002/cne.21180

103. T. K. Kim, M. Hemberg, J. M. Gray, A. M. Costa, D. M. Bear, J. Wu, D. A. Harmin, M. Laptewicz, K. Barbara-Haley, S. Kuersten, E. Markenscoff-Papadimitriou, D. Kuhl, H. Bito, P. F. Worley, G. Kreiman, M. E. Greenberg, Widespread transcription at neuronal activity-regulated enhancers. *Nature* **465**, 182–187 (2010). Medline doi:10.1038/nature09033

104. W. C. Warren, D. F. Clayton, H. Ellegren, A. P. Arnold, L. W. Hillier, A. Künstner, S. Searle, S. White, A. J. Vilella, S. Fairley, A. Heger, L. Kong, C. P. Ponting, E. D. Jarvis, C. V. Mello, P. Minx, P. Lovell, T. A. Velho, M. Ferris, C. N. Balakrishnan, S. Sinha, C. Blatti, S. E. London, Y. Li, Y. C. Lin, J. George, J. Sweedler, B. Southey, P. Gunaratne, M. Watson, K. Nam, N. Backström, L. Smeds, B. Nabholz, Y. Itoh, O. Whitney, A. R. Pfenning, J. Howard, M. Völker, B. M. Skinner, D. K. Griffin, L. Ye, W. M. McLaren, P. Flicek, V. Quesada, G. Velasco, C. Lopez-Otin, X. S. Puente, T. Olender, D. Lancet, A. F. Smit, R. Hubley, M. K. Konkel, J. A. Walker, M. A. Batzer, W. Gu, D. D. Pollock, L. Chen, Z. Cheng, E. E. Eichler, J. Stapley, J. Slate, R. Ekblom, T. Birkhead, T. Burke, D. Burt, C. Scharff, I. Adam, H. Richard, M. Sultan, A. Soldatov, H. Lehrach, S. V. Edwards, S. P. Yang, X. Li, T. Graves, L. Fulton, J. Nelson, A. Chinwalla, S. Hou, E. R. Mardis, R. K. Wilson, The genome of a songbird. *Nature* **464**, 757–762 (2010). Medline doi:10.1038/nature08819

105. R. Schippert, F. Schaeffel, M. P. Feldkaemper, Microarray analysis of retinal gene expression in Egr-1 knockout mice. *Mol. Vis.* **15**, 2720–2739 (2009). Medline

106. T. Aid-Pavlidis, P. Pavlidis, T. Timmusk, Meta-coexpression conservation analysis of microarray data: A “subset” approach provides insight into brain-derived neurotrophic factor regulation. *BMC Genomics* **10**, 420 (2009). Medline doi:10.1186/1471-2164-10-420

107. J. Boros, I. J. Donaldson, A. O'Donnell, Z. A. Odrowaz, L. Zeef, M. Lupien, C. A. Meyer, X. S. Liu, M. Brown, A. D. Sharrocks, Elucidation of the ELK1 target gene network reveals a role in the coordinate regulation of core components of the gene regulation machinery. *Genome Res.* **19**, 1963–1973 (2009). Medline doi:10.1101/gr.093047.109

108. S. Dong, K. L. Replogle, L. Hasadsri, B. S. Imai, P. M. Yau, S. Rodriguez-Zas, B. R. Southey, J. V. Sweedler, D. F. Clayton, Discrete molecular states in the brain accompany changing responses to a vocal signal. *Proc. Natl. Acad. Sci. U.S.A.* **106**, 11364–11369 (2009). Medline doi:10.1073/pnas.0812998106

109. S. W. Flavell, T. K. Kim, J. M. Gray, D. A. Harmin, M. Hemberg, E. J. Hong, E. Markenscoff-Papadimitriou, D. M. Bear, M. E. Greenberg, Genome-wide analysis of MEF2 transcriptional program reveals synaptic target genes and neuronal activity-dependent polyadenylation site selection. *Neuron* **60**, 1022–1038 (2008). Medline doi:10.1016/j.neuron.2008.11.029

110. J. Lalonde, P. E. Lachance, A. Chaudhuri, Developmental and activity-dependent genomic occupancy profiles of CREB in monkey area V1. *Genes Brain Behav.* **8**, 149–160 (2009). Medline doi:10.1111/j.1601-183X.2008.00450.x

111. M. D. Croning, M. C. Marshall, P. McLaren, J. D. Armstrong, S. G. Grant, G2Cdb: The Genes to Cognition database. *Nucleic Acids Res.* **37** (Database), D846–D851 (2009). Medline doi:10.1093/nar/gkn700

112. R. P. Haberman, H. J. Lee, C. Colantuoni, M. T. Koh, M. Gallagher, Rapid encoding of new information alters the profile of plasticity-related mRNA transcripts in the hippocampal CA3 region. *Proc. Natl. Acad. Sci. U.S.A.* **105**, 10601–10606 (2008). Medline doi:10.1073/pnas.0804292105

113. S. C. Vernes, E. Spiteri, J. Nicod, M. Groszer, J. M. Taylor, K. E. Davies, D. H. Geschwind, S. E. Fisher, High-throughput analysis of promoter occupancy reveals direct neural targets of FOXP2, a gene mutated in speech and language disorders. *Am. J. Hum. Genet.* **81**, 1232–1250 (2007). Medline doi:10.1086/522238

114. E. Spiteri, G. Konopka, G. Coppola, J. Bomar, M. Oldham, J. Ou, S. C. Vernes, S. E. Fisher, B. Ren, D. H. Geschwind, Identification of the transcriptional targets of FOXP2, a gene linked to speech and language, in developing human brain. *Am. J. Hum. Genet.* **81**, 1144–1157 (2007). Medline doi:10.1086/522237

115. A. E. McKee, N. Neretti, L. E. Carvalho, C. A. Meyer, E. A. Fox, A. S. Brodsky, P. A. Silver, Exon expression profiling reveals stimulus-mediated exon use in neural cells. *Genome Biol.* **8**, R159 (2007). Medline doi:10.1186/gb-2007-8-8-r159

116. G. Xiang, L. Pan, W. Xing, L. Zhang, L. Huang, J. Yu, R. Zhang, J. Wu, J. Cheng, Y. Zhou, Identification of activity-dependent gene expression profiles reveals specific subsets of genes induced by different routes of Ca(2+) entry in cultured rat cortical neurons. *J. Cell. Physiol.* **212**, 126–136 (2007). Medline doi:10.1002/jcp.21008

117. K. Sugino, C. M. Hempel, M. N. Miller, A. M. Hattox, P. Shapiro, C. Wu, Z. J. Huang, S. B. Nelson, Molecular taxonomy of major neuronal classes in the adult mouse forebrain. *Nat. Neurosci.* **9**, 99–107 (2006). Medline doi:10.1038/nn1618